

The Walkaway Star HP Tau/G2: Evidence for a Stellar Merger

BO REIPURTH,^{1,2} J. BALLY,³ P. FRIBERG,⁴ D. M. FAES,⁵ C. BRICEÑO,⁶ M. S. CONNELLEY,^{7,8} C. FLORES,⁹ A. M. CODY,¹⁰ AND H. ZINNECKER¹¹

¹*Institute for Astronomy, University of Hawaii at Manoa, 640 N. Aohoku Place, Hilo, HI 96720, USA*

²*Planetary Science Institute, 1700 E Fort Lowell Rd Ste 106, Tucson, AZ 85719, USA*

³*Center for Astrophysics and Space Astronomy, University of Colorado, Boulder, CO 80309, USA*

⁴*East Asian Observatory, 660 North Aohoku Place, Hilo, HI 96720, USA*

⁵*National Radio Astronomy Observatory, 1003 Lopezville Road, Socorro, NM 87801, USA*

⁶*NSF's NOIRLab/Cerro Tololo Inter-American Observatory, Casilla 603, La Serena, Chile*

⁷*Institute for Astronomy, University of Hawaii at Manoa, 640 N. Aohoku Place, HI 96720*

⁸*Staff Astronomer at the Infrared Telescope Facility, which is operated by the University of Hawaii under contract NNH14CK55B with the National Aeronautics and Space Administration*

⁹*Institute of Astronomy and Astrophysics, Academia Sinica, 11F of AS/NTU Astronomy-Mathematics Building, No.1, Sec. 4, Roosevelt Rd, Taipei 10617, Taiwan, R.O.C.*

¹⁰*SETI Institute, 339 N Bernardo Ave, Suite 200, Mountain View, CA 94043*

¹¹*Nucleo de Astroquímica y Astrofísica, Universidad Autónoma de Chile, Av. Pedro de Valdivia 425, Santiago, Chile*

ABSTRACT

HP Tau/G2 is a luminous, short-period, fast-rotating G-type weak-line T Tauri star with a large radius, an oblate shape with gravity-darkening, little circumstellar material, and centered in a slowly expanding cloud cavity. It is an X-ray source and a variable nonthermal radio source. It forms, together with the late-type T Tauri star KPNO 15, a pair of oppositely directed walkaway stars launched when a multiple system broke apart \sim 5600 yr ago. Momentum conservation indicates a mass of G2 of only \sim 0.7 M_{\odot} , much lower than \sim 1.9 M_{\odot} determined from evolutionary models. G2 is virtually a twin of FK Com, the prototype of a class of evolved stars resulting from coalescence of W UMa binaries. We suggest that G2 became a very close and highly eccentric binary during viscous evolution in the protostellar stage and with KPNO 15 formed a triple system, which again was part of a larger unstable group including the binary G3 and the single G1. Dynamical evolution led to multiple bound ejections of KPNO 15 before it finally escaped after \sim 2 Myr. As a result the G2 binary recoiled and contracted 5600 yr ago, became Darwin unstable and merged in a major outburst \sim 2000 yr ago. The nearby compact triple system G1+G3 was also disturbed, and broke up 4900 yr ago, forming another walkaway pair. The G5 star HD 283572 has similar unusual properties, indicating that G2 is not a pathological case. G2 is now fading towards a new stable configuration. YSO mergers may be rather common and could explain some FUor eruptions.

Keywords: Binary stars (254) — Multiple stars (1081) — Stellar mergers (2157) — Pre-main sequence stars (1290) — Star formation (1569) — Molecular clouds (1072) — FU Orionis stars (553)

1. INTRODUCTION

Small reflection nebulae are ubiquitous in clouds associated with star forming regions, for a catalog see T.Yu. Magakian (2003). They represent a relatively

brief stage when the outflows and winds from recently formed low mass stars break through the surface of the cloud, allowing light to flood the surroundings until the stars have drifted away or the cloud is destroyed. Most of these nebulae show very few changes on a human timescale, but some show rapid variability as circumstellar material creates a shadow play across the surrounding cloud surface (e.g., H. Knox-Shaw 1916; E.P.

Corresponding author: Bo Reipurth
 reipurth@hawaii.edu

Hubble 1916; S.E.Dahm & L.A. Hillenbrand 2017). In at least one case, the actual emergence of a reflection nebula from an embedded infrared source has been witnessed (B. Reipurth & J. Bally 1986).

The large majority of reflection nebulae are diffuse. However, a few are highly structured and display sharp edges. One such case, Magakian 77 in the L1536 cloud in Taurus, surrounds a compact group of stars known as the HP Tau group, first noted by O. Struve & W.C. Straka (1962) (Figure 1). M. Cohen & L. Kuhi (1979) found that the group consists of five young stars, HP Tau/G1, HP Tau/G2, and HP Tau/G3 (hereafter G1, G2, and G3)¹ in addition to HP Tau itself and the young H α emission star Haro 6-28. Another 7 members have subsequently been identified, see Appendix A. The group, identified in Figure 2, illuminates the large, sculpted reflection nebula. The brightest star near the center of the nebula is G2. Due to their proximity, it is often assumed that HP Tau plus G1 and G2 form a bound system, but we show here that it is not the case.

In this paper we study the structure and kinematics of the cloud around and illuminated by the HP Tau group. We determine basic properties of G2, and investigate the origin of the unusual cloud structure in the context of the chaotic evolution of a small multiple system. We argue that the properties of G2 and the structure and kinematics of the surrounding gas can be understood if G2 is a merger of two young low-mass stars, triggered by the breakup of a multiple system about 5600 yr ago.

2. OBSERVATIONS

We have observed G2 with a variety of telescopes and instruments to better understand the nature of this peculiar star.

APO: Near-infrared observations were obtained with the NICFPS camera on the Apache Point Observatory 3.5 meter telescope. NICFPS uses a 1024×1024 pixel Rockwell Hawaii 1-RG HgCdTe detector. The pixel scale is $0.273''$ per pixel with a field of view $4.58''$ on a side. Multiple images with 180 second exposures were obtained in the $2.122 \mu\text{m}$ S(1) line of H $_2$ using a narrow-band filter (FWHM= 0.4% of the central wavelength). Visual wavelength images were obtained using the ARCTIC CCD camera which has an $8'$ field of view. Images were obtained in the broad-band SDSS g, r, and i filters and with 80\AA passband narrow-band filters centered on the 6563\AA H α emission line and on the $\lambda\lambda 6717 / 6731\text{\AA}$ [S II] doublet. Three exposures were obtained in each filter with durations of 60 seconds per exposure in the

broad-band filters and 600 seconds in the narrow-band filters.

SOAR: The optical spectra were acquired the night of UT2024-01-26 with the Goodman High Throughput Spectrograph (J. Clemens et al. 2004), installed on the SOAR 4.1m telescope on Cerro Pachón, Chile. We used the 400 1/mm grating in its 400M1, and 400M2 + GG 455 filter, preset modes, with 2×2 binning. These two configurations combined span the wavelength range $\sim 3600 \lesssim \lambda \lesssim 9000 \text{\AA}$. We used the $1''$ wide long slit, which results in a FWHM resolution = 6.7\AA (equivalent to $R = 830$). We used exposure times of 300s for all targets. For HP Tau, we obtained 3×300 s spectra in the 400M2 and 1×300 s spectrum in the 400M1 mode. For HP Tau/G1 and KPNO Tau-15 we obtained a 1×300 s spectrum in each 400M1 and 400M1 mode.

The near-infrared spectra of HP Tau, HP Tau/G1, and KPNO Tau-15 were obtained on UT2024-01-25 using the TripleSpec 4.1 near-IR spectrograph at the SOAR telescope. We observed an A0 star at the same airmass as each of the three targets, in order to perform the telluric correction. The data were reduced with the Spextool IDL package (M. Cushing et al. 2004).

SpeX: Observations were carried out with the 3.2 m NASA Infrared Telescope Facility (IRTF) on Maunakea, Hawaii with SpeX. SpeX was used in the short cross-dispersed mode, covering $0.7 \mu\text{m}$ to $2.5 \mu\text{m}$. We used the $0.5''$ wide slit, yielding a resolving power of $R=1200$. Stars were nodded along the slit, with two exposures taken at each nod position in the usual ABBA beam switch pattern. An A0 telluric standard star was observed at the same air mass as the target and within a half-hour. A thorium-argon lamp was observed for wavelength calibration and a quartz lamp for flat fielding. An arc/flat calibration set was observed for each target/standard pair. The data were obtained on Sept 30, 2019, October 1, 2019, and Oct 15, 2019, and were reduced using *Spextool*. JHKL aperture photometry was obtained on September 30, 2019.

iSHELL: We observed HP Tau G2 on October 23, 2020, using the high-resolution near-infrared echelle spectrograph iSHELL on the IRTF (J. Rayner et al. 2022).

The observations were performed in the K2 mode, covering the range from 2.09 to $2.38 \mu\text{m}$, using the 0.75 arcsecond slit to achieve a spectral resolution of $R \sim 50,000$.

JCMT: The $J=3-2$ ^{12}CO and ^{13}CO at 345 and 330 GHz were observed with the 15-meter JCMT using the 16 channel HARP receiver and the ACSIS correlator. The ^{12}CO observations cover an $850''$ (east to west) by $830''$ (north to south) field centered on HP Tau. The bulk of the ^{12}CO data was obtained in the fall of 2019

¹ These systems are also known as CoKu HP Tau G1/G2/G3



Figure 1. The large highly structured reflection nebula Magakian 77 surrounds the little group of young stars including HP Tau. The figure is almost 8 arcmin wide. This is a 13hr 20min exposure with a 1m telescope through B, G, R filters plus luminance. Courtesy Alexandre Zaytsev and Mark Hanson.

with some additional data obtained in 2023. The ^{13}CO observations cover an 800'' (east to west) by 600'' (north to south) field. While some ^{13}CO data was obtained in 2019 the bulk was observed in 2023. The beam size is about 15''. The spectral resolution of the ^{12}CO observations were 0.025 km s $^{-1}$ while the spectral resolution of the ^{13}CO observations were 0.055 km s $^{-1}$. This intrinsic resolution has been smoothed as specified in the maps and spectra presented.

3. THE YOUNG STARS AROUND HP TAU

HP Tau is a young H α emission star associated with the L1536 cloud, located in the southern part of the Taurus complex of star forming clouds. Figure 2-top identifies the 12 known young low-mass stars and brown dwarfs that are within 7.5 arcmin from HP Tau. This is one of the most compact aggregates in Taurus (K.L. Luhman 2018) and is part of a more scattered distribution over $\sim 3^\circ$ of more than 30 young stars that share broadly common motions (K.L. Luhman 2023).

The properties of these 12 stars and brown dwarfs (some of which are binaries) are listed in Table 1. G2, KPNO Tau-15 (throughout the following called KPNO 15), G1, and HP Tau are discussed in detail in Section 4. Additional information on the other 8 stars is given in Appendix A. Most of the stars have near-

infrared excesses or other evidence for circumstellar material. (Figure 2-bottom).

Table 1 lists the Gaia DR3 proper motions for confirmed members of the HP Tau group. We have selected the six stars that have distance uncertainties of less than ± 1.6 pc: HP Tau, G1, G3, KPNO 15, XEST 08-049, and FF Tau. These data suggest a distance to the HP Tau group of 162.6 ± 0.6 pc, which is consistent within the errors to the VLBA distance for G2 of 161.2 ± 0.9 pc by R.M. Torres et al. (2009) and the VLBI distance for G2 of 162.7 ± 0.8 pc by P. Galli et al. (2018). The weighted mean of these three distance estimates is 162.2 ± 0.4 pc, which we adopt for the HP Tau group.

A number of studies have explored the star formation history of the Taurus young star population. D.M. Krokowski et al. (2021) estimated the age of the young stars associated with the L1536 cloud, which includes the HP Tau group, as $2.01_{-0.29}^{+0.32}$ Myr. R. Kerr et al. (2021) determined an age of 3.3 ± 0.9 Myr, and finally K.L. Luhman (2023) suggested $2.1_{-1.4}^{+4.0}$ Myr. We here adopt the more precise age estimate of 2.0 ± 0.3 Myr for the group.

Table 1. Young Stars in the HP Tau Group

#	Object	2MASS	SpT ^a	G	J ^b	H ^b	K ^b	pmra ^c	pmdec ^c	Notes
				[mag]	[mag]	[mag]	[mag]	[mas/yr]	[mas/yr]	
1	FF Tau	J04352089+2254242	K8	12.78 0.02	9.78 0.02	8.93 0.02	8.59 0.02	9.97 0.03	-19.14 0.03	Binary 36 mas ^d
2	XEST 08-049	J04355286+2250585	M4.25	14.72 0.03	10.93 0.01	10.17 0.01	9.71 0.04	10.55 0.06	-16.93 0.04	
3	HQ Tau	J04354733+2250216	K2	11.53 0.03	8.85 0.02	8.01 0.02	7.42 0.02	10.87 0.24	-18.98 0.18	Spec. Binary ^e
4	KPNO 15	J04355109+2252401	M2.75	14.73 0.03	11.30 0.01	10.42 0.01	10.08 0.03	6.10 0.04	-28.13 0.03	Walkaway star
5	KPNO 9	J04355143+2249119	M8.5V	20.57 0.04	15.48 0.04	14.66 0.04	14.19 0.05	11.12 1.59	-15.04 1.10	Brown dwarf
6	XEST 08-033	J04354203+2252226	M4.75	15.31 0.05	11.25 0.01	10.45 0.04	9.97 0.04	10.02 0.07	-16.89 0.05	
7	HP Tau/G1	J04355209+2255039	M4.5	15.47 0.02	11.31 0.02	10.23 0.02	9.81 0.02	7.23 0.08	-7.65 0.05	Walkaway star
8	HP Tau	J04355277+2254231	K4.0	13.03 0.08	9.36 0.01	8.35 0.06	7.64 0.06	9.04 0.06	-13.85 0.05	Binary 17 mas ^f
9	HP Tau/G3	J04355349+2254089	M0.6	13.32 0.07	9.80 0.02	9.05 0.05	8.75 0.05	11.67 0.05	-18.76 0.03	Binary 31 mas ^g
10	HP Tau/G2	J04355415+2254134	G2	10.51 0.05	8.25 0.02	7.57 0.04	7.38 0.04	13.46 0.07	-11.40 0.05	Walkaway star
11	Haro 6-28	J04355684+2254360	M3.1	14.95 0.05	11.08 0.01	10.15 0.03	9.53 0.03	10.56 0.36	-17.13 0.24	Binary 0.66" ^h
12		J04355760+2253574	M5	19.91 0.09	15.06 0.02	14.06 0.03	13.47 0.03			

NOTE— (a): #1,3,8,9,10,11 G.J. Herczeg & L.A. Hillenbrand (2014) #2,6,7 K.L. Luhman et al. (2009) #4 K.L. Luhman et al. (2003) #5 C. Briceño et al. (2002) #12 K.L. Luhman et al. (2017) (b): The JHK photometry is in the MKO system. The values for FF Tau, KPNO 9, and G1 are transformed from 2MASS using the transformations of M.S. Connelley et al. (2007) (c): Proper motions from Gaia DR3. (d): M. Simon et al. (1987) (e): G.J. Herczeg & L.A. Hillenbrand (2014) suggest that HQ Tau is a spectroscopic binary, which is confirmed by Gaia’s very large RUWE value. (f): A. Richichi et al. (1994) (g): A.C. Rizzuto et al. (2020) (h): Ch. Leinert et al. (1993)

A.C. Rizzuto et al. (2020) used non-redundant aperture masking interferometry with NIRC2 on the Keck-II telescope and presented orbits and dynamical masses for the two binaries G3 (P~27 yr) and FF Tau (P~15 yr). They estimated ages for the primary components of ~3 Myr, but the secondaries have ages half of that.

4. GAIA PROPER MOTIONS: WALKAWAY STARS

A. Blaauw (1961) identified a number of high-velocity OB stars, which he assumed had been ejected from their regions of birth. For those with a velocity larger than 30 km s⁻¹ he coined the term runaway stars. Since then it has been estimated that roughly 10-30% of O stars and about 2-10% of B stars have such high velocities, dependent on different definitions of runaway stars (e.g., M. Renzo et al. 2019). It was predicted that young low-mass runaways would also be discovered (M.F. Sterzik & R.H. Durisen 1995; C. Schoettler et al. 2019) but only recently have the first of this population been identified,

(e.g., A. McBride & M. Kounkel 2019; J. Farias et al. 2020; I. Platais et al. 2020).

Eldridge et al. (2011) analyzed the distribution of runaway velocities for massive stars and proposed to include also slower ejectees with a lower limit of 5 km s⁻¹. It has been suggested to use the term walkaway stars for velocities between 5 and 30 km s⁻¹ (S.E. de Mink et al. 2014).

K.L. Luhman (2018) studied the motion of the Taurus stars with Gaia DR2 data, and made the remarkable discovery that three stars in the HP Tau group, KPNO 15, G2, and G1 (the latter labeled in the Luhman paper as 2MASS J04355209+2255039) are high proper motion stars, and he suggested that G1 and KPNO 15 were once part of a multiple system that broke up about 7,200 yr ago. These conclusions were based on Gaia DR2 data, and we have revisited the proper motions using the newer Gaia DR3 data. The improvement from DR2 to DR3 is significant. But an uncertainty for interpretation

Table 2. Proper Motions within Rest Frame^a and Radial and Space Velocities

Object	Dist.	pmra	pmdec	Tang.Vel.	PA	Rad.Vel. ^b	Spa.Vel. ^c	RUWE ^d
	[pc]	[mas/yr]	[mas/yr]	[km/sec]	[deg.]	[km/sec]	[km/sec]	
FF Tau	161.0/0.8	-0.55	-1.03	0.9	~208	16.9	0.9	1.48
XEST 08-049	162.3/1.2	+0.03	+1.18	0.9	~89	17.7	1.3	1.24
HQ Tau	161.3/6.3	+0.35	-0.87	0.7	~158	16.8	0.7	13.39
KPNO 15	160.5/0.8	-4.42	-10.02	8.4	~204	12.9	9.3	1.10
KPNO 9	155.8/27	+0.60	+3.07	2.4	~11	..		1.20
XEST 08-033	164.2/1.6	-0.50	+1.22	1.0	~337	16.8	1.0	1.06
HP Tau/G1	160.8/1.5	-3.29	+10.46	8.5	~343	1.4	17.5	1.18
HP Tau	171.2/1.5	-1.48	+4.26	3.5	~341	..		2.77
HP Tau/G3	159.5/1.0	+1.15	-0.65	1.0	~119	..		2.43
HP Tau/G2	167.2/1.7	+2.94	+6.71	5.7	~24	16.6	5.7	3.85
Haro 6-28	149.0/6.5	-0.99	+0.98	1.1	~315	16.6	1.1	10.04

NOTE—(a): The rest frame is 10.52 mas/yr, -18.11 mas/yr

(b): The radial velocities listed are heliocentric and are from APOGEE2 (H.J. Jönsson et al. 2020), except for G2 which is from D.C. Nguyen et al. (2012). The uncertainty for G1 is larger, about ± 7 km s⁻¹.

(c): Formal values of the space velocities are given in the rest frame of the cloud with uncertainties of a few km s⁻¹ except for G1 (see note b). The heliocentric velocity of the cloud is 16.7 km s⁻¹. (d): Gaia Renormalized Unit Weight Error; a large value indicates the presence of a very close companion

comes from transforming the observed proper motions to the peculiar velocity frame of the little compact group of YSOs around HP Tau. The reference frame obviously does not affect the relative motions of the stars, but the *relative* sizes of the vectors depend on the reference frame, and thus will impact stellar masses derived from momentum conservation. K.L. Luhman (2023) obtained the mean motion of many stars in the whole L1536 complex, finding a group velocity of 10.3, -17.0 mas/yr in α and δ . In Appendix B we discuss this further.

We have chosen to use only the YSOs immediately around HP Tau within a radius of 7.5 arcmin. These are the 12 stars listed in Table 1. Of the 11 members with Gaia measurements, four stars - G1, G2, KPNO 15, and HP Tau - have higher proper motions and are known or suspected walkaway stars and as such are not included in the determination of the rest frame. We calculate a weighted mean proper motion of the remaining 7 stars of 10.52, -18.11 mas/yr. Table 2 lists the motions of the individual members of the HP Tau group when corrected for this group motion.

We note that in the past G2 and KPNO 15 were once close to each other. In the reference frame we determined, the vectors of G2 and KPNO 15 are pointing in opposite directions to within 0.6°, as must be the case if one recoiled from the other, see Figure 3. With the current (DR3) accuracy of the Gaia astrometry the two

stars were within 1.1'' of each other ~5600 yr ago (at the 2000-position 4:35:52.2 +22:53:36). If they broke up it implies that one of the two is a binary.

The tangential velocity of G2 (5.65 km s⁻¹) is less than that of KPNO 15 (8.44 km s⁻¹) by a factor of ~ 0.67 so from momentum conservation it follows that in this reference frame G2 must be more massive than KPNO 15 by a factor of ~ 1.5 , which is consistent with G2 having an earlier spectral type than KPNO 15.

R.M. Torres et al. (2009) measured a heliocentric radial velocity for G2 of $+17.7 \pm 1.0$ km s⁻¹. D.C. Nguyen et al. (2012) found $+16.6 \pm 1.0$ km s⁻¹, and J.L. Rivera et al. (2015) determined 16.6 ± 1.7 km s⁻¹. Gaia DR3 lists a velocity of 23.0 km s⁻¹, but without an error estimate. The weighted mean of the Torres, Nguyen, and Rivera values is 17.0 ± 0.7 km s⁻¹. H.J. Jönsson et al. (2020) included KPNO 15 in their catalog of radial velocities from the APOGEE2 DR16 survey and found a radial velocity of 12.86 km s⁻¹. The heliocentric radial velocity of the cloud from CO data is 16.7 km s⁻¹ (see Section 9) and if we allow an error not exceeding 0.7 km s⁻¹ for each of these three numbers, we find that - within the resulting range of possible angles - for an assumed angle to the plane of the sky of $\sim 16^\circ$, the two stars would move precisely in opposite directions, with G2 being redshifted and KPNO 15 blueshifted.

This scenario does not explain the large velocity of the walkaway star G1. The star has a tangential velocity of

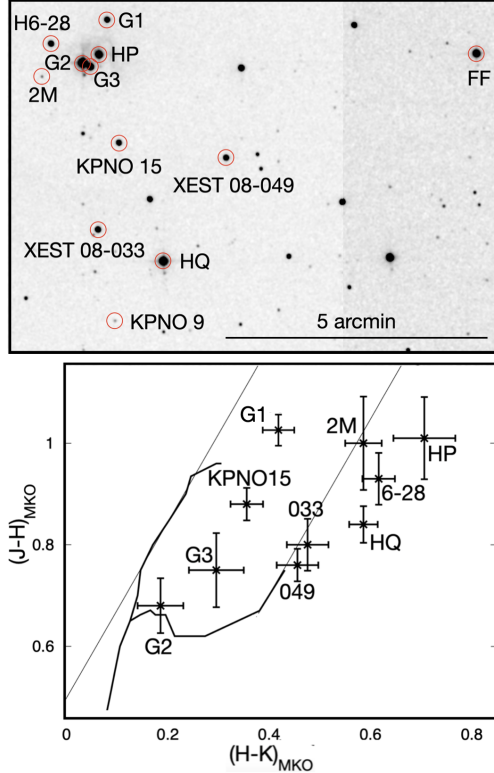


Figure 2. (top) The YSOs within the Magakian 77 reflection nebula are identified in this 2MASS K-band image, and their properties are listed in Table 1. H6-28 is Haro 6-28 and 2M is 2MASS J04355760+2223574. FF Tau is outside the field to the west. North is up and east is left. (bottom) A J-H vs H-K color-color diagram of ten of the sources in the HP Tau multiple system. The dwarf and giant loci are from M.S. Bessell & J.M. Brett (1988) and the reddening lines from G.H. Rieke & Lebofsky (1985). The abbreviations refer to the names in Table 1.

8.5 km s⁻¹ and Gaia DR3 lists a heliocentric radial velocity of 1.4±6.9 km s⁻¹. Given the heliocentric velocity of the gas of 16.7 km s⁻¹ it follows that G1 has a space velocity of about 17.5±7 km s⁻¹.

To explain this peculiar motion we would expect to find a counterpart moving in the opposite direction. However, we have searched the Gaia DR3 catalog for a walkaway star moving precisely away from G1, but within errors no plausible candidate was found.

Within errors, however, G1 is moving straight away from G3. Since it is the only young star in the path of G1, it is a possible candidate for pairing with G1, see Figure 3. The problem is that the proper motions of G3 are at a ~45 degree angle to the motion of G1. But G3 is a 31 mas binary (A.C. Rizzuto et al. 2020), which could easily affect the Gaia proper motions. The angular separation of G1 and G3 is 58 arcsec, and at the relative speeds of G1 and G3 this implies a travel time

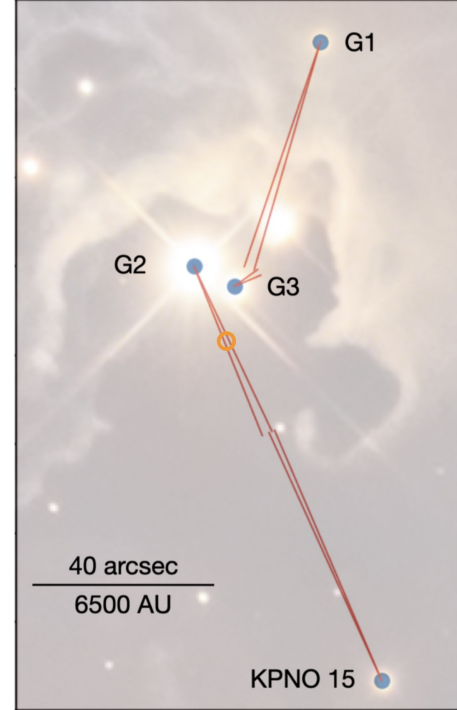


Figure 3. The relative proper motions of the stars G2, KPNO 15, G1, and G3 in a reference system based on 7 stars from the surrounding group. G2 and KPNO 15 were within one arcsecond of each other about 5600 yr ago. G1 is another walkaway star, possibly related to the binary G3. The orange circle marks the approximate center of the inner rim of the cavity and the presumed site of the merger, suggesting it happened roughly 2000 yr ago.

of roughly 4700 yr. So if G1 was once bound to G3, then they broke apart less than 1000 yr after the breakup of G2 and KPNO 15.

The unsatisfactory aspect of this scenario is that it requires two nearby but apparently independent triple systems to each break apart within a few thousand years, which is statistically unlikely, unless there is some connection between the two systems. We have instead considered whether the three stars could have originated from the breakup of a single multiple system. However, even with a generous interpretation of the Gaia errors, there is no solution where the three stars were at the same point at the same time and maintained momentum conservation.

In Section 7.4 we discuss a possible dynamical history of the small aggregate of young stars surrounding G2.

5. THE WALKAWAY STARS

We here discuss what is known about each of the three stars with anomalous velocities.

5.1. The Walkaway Star G2

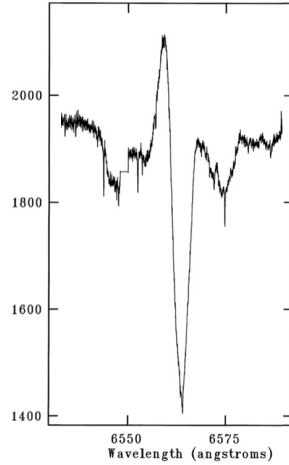


Figure 4. HIRES spectrum taken on Dec 21, 2005 by George Herbig showing the $H\alpha$ emission line profile of G2 overlaid a very broad absorption line with a width of $\sim 1200 \text{ km s}^{-1}$. The central absorption is likely formed by the superposition of two blue and red-shifted emission peaks that vary in anti-phase, causing the central dip to move back and forth, see Section 5.1.

G2 is generally classified as a G2 star (e.g., P. Hartigan et al. 1994; G.J. Herczeg & L.A. Hillenbrand 2014), but sometimes also as G0 (e.g., M. Cohen & L. Kuhi 1979; K.L. Luhman et al. 2010). A low-resolution spectrum from LAMOST shows a G-type spectrum, but peaking around 8000 Å, indicating extinction. Indeed G.J. Herczeg & L.A. Hillenbrand (2014) determine an $A_V = 2.55 \pm 0.2$. G2 is not a known $H\alpha$ emission star, but a spectrum from George Herbig's archives reveals a very wide $\sim 1200 \text{ km s}^{-1}$ absorption line overlaid with a double-peaked emission (Figure 4). Given the absence of detectable circumstellar material (see below), the absorption component is unlikely to be due to accretion. From comparison with the star FK Com (see Section 7.3.2) it is well explained as the result of a very strong and broad $H\alpha$ line ($\sim 1200 \text{ km s}^{-1}$) overlaid with a double-peaked emission line whose blue and red components vary in anti-phase, leading to the central absorption to shift back and forth.

A 2.0 - 2.4 μm SpeX spectrum of the star shows no evidence for a near-infrared excess that could indicate the presence of a circumstellar disk. Figure 5 shows a comparison with the G2IV standard star HD 126868 to which an extinction $A_V=2.0$ has been applied.

Our near-infrared photometry also shows that G2 has no near-infrared excess (Figure 2) and the energy distribution of G2 based on WISE photometry shows a clean Planck curve at least out to about 22 μm . A small excess is seen with Spitzer at 70 and 160 μm , but at those wavelengths the point spread function is so large that

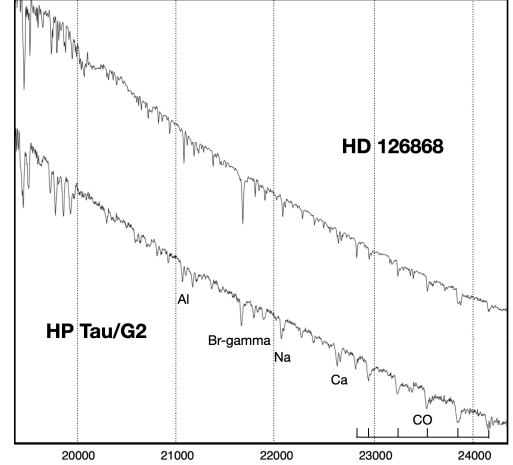


Figure 5. Comparison of the 2.0 - 2.4 μm SpeX spectrum of G2 and the G2IV standard star HD 126868 with an extinction of $A_V=2.0$ applied. The spectra confirm G2's spectral type as G2 with very minor differences apart from the faster rotation of G2. The abscissa is wavelength in Angstroms.

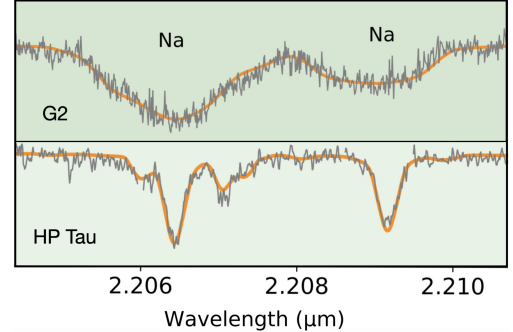


Figure 6. Part of an iSHELL spectrum of HP Tau/G2 and HP Tau with $vsini$ of $\sim 130 \text{ km s}^{-1}$ and 17 km s^{-1} , respectively. The rotational line broadening is evident. The spectra have been shifted to the same velocity.

it includes the T Tauri stars G3 and HP Tau which are only 10'' and 21'' away, respectively. A. Garufi et al. (2024) puts an upper limit on any disk of G2 of at most 1 M_\oplus of dust. In Section 7 we discuss a mechanism that would remove any remnant disk material.

We have obtained a high resolution spectrum in the wavelength range from 2.107 to 2.304 μm with iSHELL on the IRTF 3m telescope, part of which is seen in Figure 6, and as is obvious from the line profiles, G2 is a fast rotator. We measure a $vsini$ of $\sim 130 \text{ km s}^{-1}$, (see Section 6.3), which confirms the extreme rotational velocity of $\sim 100 \pm 20 \text{ km s}^{-1}$ measured by L. Hartmann et al. (1986) and $127 \pm 4 \text{ km s}^{-1}$ by D.C. Nguyen et al. (2012). This makes G2 one of the faster known rotating low-mass young stars, (e.g., L. Malo et al. 2014).

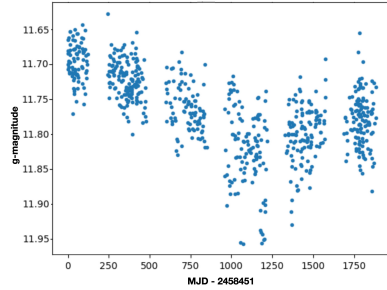


Figure 7. The g light curve of HP Tau G2 from Nov 28, 2018 to Jan 16, 2024 as observed by the ASAS-SN survey (Shappee et al. 2014, Kochanek et al. 2017).

G2 is an X-ray source: XEST 08-051 (M. Güdel et al. 2007), and J.H. Bieging et al. (1984) found it to be a point-like non-thermal radio source, with significant variability at 15 and 5 GHz (M. Cohen & J. Bieging 1986; D. O’Neal et al. 1990). This is unusual, since radio emission from low-mass young stars is generally found to be thermal (e.g., G. Anglada 1996) and indicative of partially ionized outflows (S.P. Reynolds 1986). A few objects are known to emit synchrotron radiation, (e.g., L.F. Rodriguez et al. 1989; T.P. Ray et al. 1997; S.J.D. Purser et al. 2018), which is ascribed to diffusive shock acceleration of electrons to mildly relativistic velocities in a highly supersonic flow of turbulent magnetized plasma where it interacts with the ambient medium (e.g., R.N. Henriksen et al. 1991; S. Mohan et al. 2022).

G2 is a variable star named V1025 Tau. The ASAS-SN g -light curve from Nov 28, 2018 to Jan 16, 2024 in Figure 7 shows a low-amplitude irregular variability within a range of 0.5 mag. based on g -photometry from multiple sites. There appears to be a long term undulation in the light curve, and if it is periodic then the period would be at least 6.5 years. This might then represent the activity cycle of the star. The ASAS-SN point spread function is about 15 arcsec, and as previously noted G3 is 10 arcsec away, hence any variability of G3 could in principle affect the photometry. However, G3 is more than 3 1/2 magnitudes fainter in V, so the impact would be minimal.

G2 has a well determined and stable rotational period of 1.2d which was first measured by F.J. Vrba et al. (1989) and later confirmed by J. Bouvier et al. (1995), L.M. Rebull et al. (2004), and M. Güdel et al. (2007). A light curve is shown in Figure 8, which shows subtle changes ascribed to star spots. L.M. Rebull et al. (2020) and A.M. Cody et al. (2022) have used K2 data to measure two well-determined simultaneous periods, $P1=1.1978d$ and $1.2222d$, with $P2/P1=1.02$, which we discuss in Appendix C.

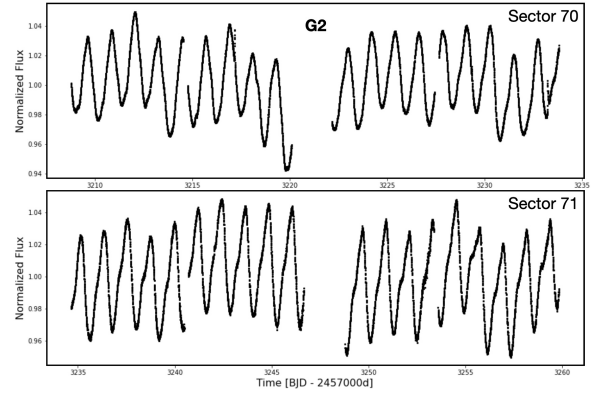


Figure 8. G2 was observed by TESS in Sectors 70 and 71 in October 2023. The observations confirm the well established period of 1.2 days. The variable asymmetries indicate the presence of large star spots. A couple of flares are detected in Sector 70.

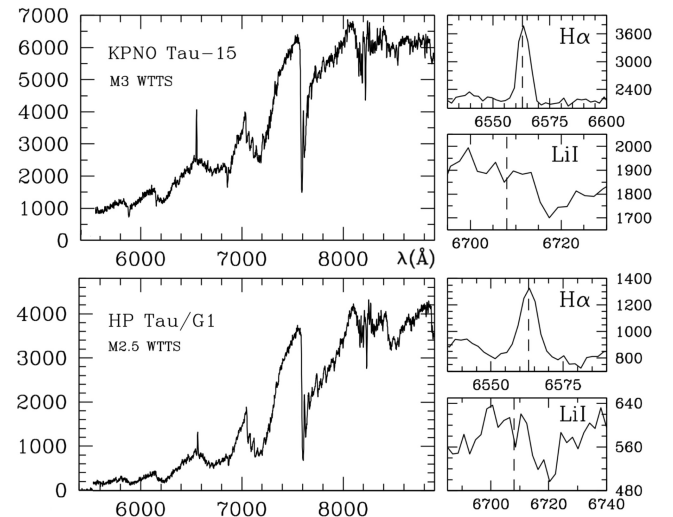


Figure 9. Low-resolution optical spectra of KPNO 15 and G1 show that both stars are weakline T Tauri stars with lithium in their spectra. The axes are counts against wavelength.

G2 was observed in a high-contrast polarization imaging study by A. Garufi et al. (2024) and it was the only star in their sample of 41 YSOs in Taurus for which a disk was not observed. G. Duvert et al. (2000) observed it with the IRAM Plateau de Bure interferometer in the $1.3 \mu\text{m}$ continuum, and detected no emission in a $3''$ beam with a 3σ detection limit of ~ 2.5 mJy. Unfortunately, at the time of writing G2 has not been observed with ALMA. So there is no direct evidence for any circumstellar material.

A. Richichi et al. (1994) used lunar occultations to search for a companion to G2, and put an upper separation limit (perpendicular to the lunar horizon) of about

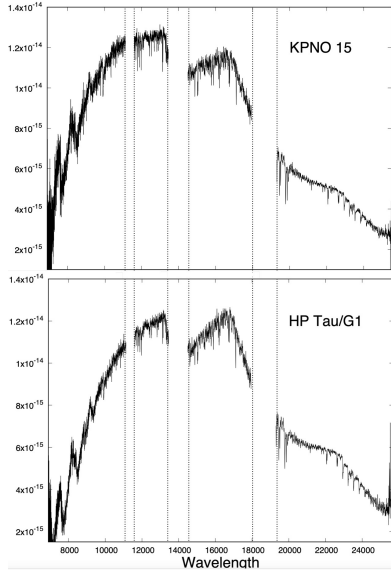


Figure 10. Low-resolution near-infrared spectra of KPNO 15 and G1 which show that they have very late spectral types and thus very low masses.

1.6 mas (about 0.2 AU) on any equally bright companion. [A.L. Kraus et al. \(2011\)](#) used non-redundant aperture masking at the Keck telescope, and the observations are sensitive to equal brightness companions at separations less than ~ 10 mas (~ 2 AU) and can detect companions 5-6 magnitudes fainter at separations larger than ~ 40 mas (~ 8 AU). The observations were able to detect companions out to a distance of 0.36 arcsec, but none were found. Kraus et al. additionally used AO observations and also found no companion in the range ~ 0.3 - 2 arcsec and flux ratios ≤ 2.5 .

We have examined archival HST images of G2 and find a very faint star 2.5 arcsec ESE of G2, which we confirmed on unpublished archival images from SPHERE (PI: Ginski). Nothing is known about it and while in principle it could be a companion to G2, it is more likely to be a background star because G2 is located in a cavity in the cloud where other background stars can be seen, see Figure 21. Future proper motion measurements will clarify this.

Gaia provides two parameters that in most cases can be indicative of the presence of a close companion, these are the renormalized unit weight error (RUWE), which evaluates whether a given star is a clean point source, and `ipd_frac_multi_peak` which is the fraction of observations for which the algorithm identified a double peak. High values of RUWE indicate probable binarity, with some authors using a limit of 1.2, others 1.4, and some 2.0. For G2 the RUWE is 3.84. But `ipd_frac_multi_peak` is 0. There are several secondary indicators of binarity,

but only one of those points to G2 being a binary ([C. Cifuentes et al. 2025](#)).

Circumstellar disks can increase the value of RUWE, (e.g., [S. Fitton et al. 2022](#)), but G2 has very little or no circumstellar material. We therefore in the following assume that G2 may have a very close, dim companion, so far only detected by Gaia.

5.2. The Walkaway Star KPNO 15

KPNO 15 was identified as a weakline T Tauri star by [K.L. Luhman et al. \(2003\)](#), who classified it as M2.75 (the full identification in SIMBAD is [BLH2002] KPNO-Tau 15). We have obtained low-resolution optical spectra of KPNO 15 (Figure 9-top), and by comparing with spectra of already known M-type TTS from the extensive sample of [Briceño et al. \(2019\)](#) we determine a spectral type of M3 for KPNO 15, with an overall uncertainty of 1 subclass, in agreement with Luhman. Gaia indicates an effective temperature of 3716 K, which corresponds to M1 in the spectral-type to T_{eff} conversions of [K.L. Luhman et al. \(2003\)](#) and [G.J. Herczeg & L.A. Hillenbrand \(2014\)](#). We also obtained a near-infrared spectrum which displays metal absorption lines and CO bands and a triangular H-band continuum due to water absorption, consistent with the optical late spectral type (Figure 10-top). Comparison with a second near-infrared spectrum taken 4 years later shows weak emission at $Br\gamma$, indicating occasional accretion. KPNO 15 is an X-ray source cataloged as XEST 08-043 ([M. Güdel et al. 2007](#)). Our JHK-photometry in Table 1 shows that KPNO 15 does not have a near-infrared excess (Figure 2-bottom). KPNO 15 was observed by TESS in Sectors 70 and 71, and we created a light curve from full frame image files (30 minute cadence) using the `lightkurve` package ([Lightkurve Collaboration et al. 2018](#)) and a custom 2×2 pixel aperture. The resulting light curve was corrected for scattered light systematics using the `lightkurve` linear regression corrector. We observe modest variability with an amplitude of about 0.05 mag (Figure 11). Running a Fourier transform periodogram we estimate a period of $\sim 5.0 \pm 0.7$ days. We note that no evidence was found for a second period that could have indicated the presence of a companion. A small flare was seen in Sector 70, but a major flare was observed in Sector 71, doubling the brightness of KPNO 15 and with a duration of over 6 hours. For a young M3 dwarf a flare that doubles the brightness of the star in the TESS bandpass would have an energy of about $10^{35.5}$ erg, which corresponds to a 'superflare' ([V. Vasilyev et al. 2024](#)) and a characteristic waiting-time between events of 1000 days (Ward Howard, pers. comm.). For a typical TESS sector of 27d duration, this

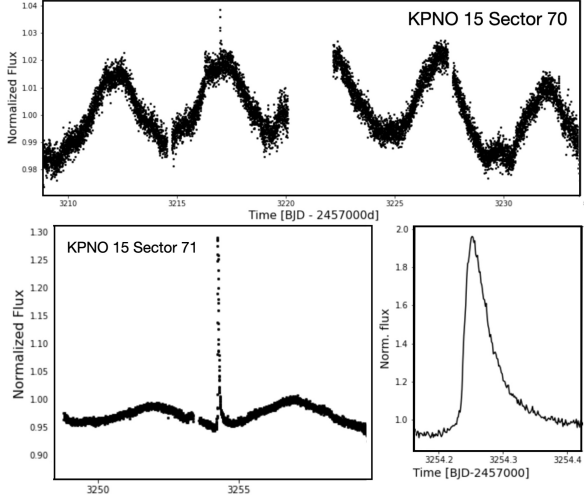


Figure 11. The TESS light curve of KPNO 15 as observed in Sector 70 and 71. KPNO 15 is a well-behaved rotationally modulated source with a period of ~ 5 days. A major flare doubling the brightness of KPNO 15 was observed in Sector 71.

suggests that one flare of this strength will be seen once every 37 sectors, i.e., it is very rare.

5.3. The Walkaway Star G1

G1, also known as 2MASS J04355209+2255039, was identified as a young H α emission star by [M. Cohen & L. Kuhi \(1979\)](#), and as an X-ray source by [M. Güdel et al. \(2007\)](#). [K.L. Luhman \(2018\)](#) found it to have a large proper motion, and suggested that it is a walkaway star. We have obtained a low-resolution optical spectrum of G1 (see Figure 9-bottom). G1 is a weakline T Tauri star which exhibits a clear Li I 6708Å absorption line, with $W(\text{Li I}) \sim 0.3\text{\AA}$. Our low-resolution near-infrared spectrum shows a spectral type slightly later than KPNO 15, and we concur with the spectral type of M4.5 assigned by [K.L. Luhman et al. \(2009\)](#). Comparison with a second near-infrared spectrum taken 4 years later shows very weak Brackett γ emission, indicative of some weak accretion (Figure 10-bottom). Our near-infrared photometry indicates a modest near-infrared excess (Figure 2-bottom).

[A.M. Cody et al. \(2022\)](#) observed G1 with K2 and found it to be a low-amplitude periodic variable with a period of 0.853 days. Clearly G1 is a very fast rotator.

6. PHYSICAL PARAMETERS OF G2

In the preceding sections we have presented all current information, from our own data as well as from the literature, on the three walkaway stars. In the following we use the available observations in an attempt to understand the nature of the peculiar star G2.

6.1. Age and Mass of G2

[A.C. Rizzuto et al. \(2020\)](#) used the effective temperature and luminosity of G2 as determined by [G.J. Herczeg & L.A. Hillenbrand \(2014\)](#) to compare with non-magnetic evolutionary models, indicating a high age of ~ 5 Myr, which is significantly older than what the authors determined for two young binaries (G3 and FF Tau) in the same little HP Tau group (~ 2.0 Myr). [A. Garufi et al. \(2024\)](#) suggest an age in the range 3.6 - 5.0 Myr.

[D.J. Mullan & J. MacDonald \(2020\)](#) followed up on this puzzling result and considered both non-magnetic and magnetic models. For the former they found an age of G2 of 4.5 Myr and a mass of $1.9 M_{\odot}$. For the latter they found that a magnetic field gives an even larger age and mass.

It is highly unlikely that G2, as part of the little HP Tau group, should have an age significantly higher than the other members of the group for which [D.M. Krolkowski et al. \(2021\)](#) determined an age of 2.0 ± 0.3 Myr (see Section 3), and we show in Section 7 that the peculiarities of G2 cause the very high ages. In the following we adopt 2 Myr as the age of G2.

[R.M. Torres et al. \(2009\)](#) used their accurate VLBA distance measurement for G2 to refine its position in the H-R diagram and compare it with four different stellar evolutionary models. The models agree that G2 has a mass between 1.7 and $1.9 M_{\odot}$. [A. Garufi et al. \(2024\)](#) suggest a mass of $2 M_{\odot}$. However, as will be discussed in Section 7, it is declining from a major outburst, which makes it appear hotter and more luminous. The fact that G2 was ejected when a triple system including KPNO 15 broke up places some useful constraints on the mass of G2. As discussed in Section 4 conservation of momentum considerations imply that the ratio of masses of G2 to KPNO 15 is about 1.5. All we know about KPNO 15 is that it has an $\sim M3$ spectral type. Evolutionary models from [I. Baraffe et al. \(2015\)](#) then suggest a mass for KPNO 15 of $\sim 0.36 M_{\odot}$. [K.L. Luhman \(2025\)](#) has established a relation between spectral type and mass for young low mass stars based on dynamical masses determined from binary orbits or rotation of circumstellar disks, and using that it follows that KPNO 15 has a probable mass of $\sim 0.45 \pm 0.2 M_{\odot}$. Relying more on the empirical relation we then adopt a mass for G2 of $\sim 0.7 M_{\odot}$, while keeping the uncertainties in mind. One or the other of the components of a disrupted triple system must be a binary. If G2 is an unresolved binary with identical components, then they would be mid-M-dwarfs, which is inconsistent with the optical spectral type. If instead KPNO 15 is an unresolved twin binary with a combined mass of $\sim 0.9 M_{\odot}$

then G2 could, at least in principle, have a mass as high as $\sim 1.3 M_{\odot}$. However, it is usually the lowest mass member of a multiple system that is ejected, and hence it is most probable that KPNO 15 is single, which we assume in the following.

6.2. Radius, Inclination, and Shape of G2

For G2 we have both a rotational velocity $v \sin i \sim 130 \text{ km s}^{-1}$ and a rotation period of 1.2 days, and that yields $r \sin i = 3.1 R_{\odot}$. This is a lower limit to R_* , primarily because of the unknown inclination angle of the star, but also because we do not know the latitude of the spot groups, and G2 is likely to rotate differentially.

[W. Herbst \(1986\)](#) and [Wm. Bruce Weaver \(1987\)](#) used the Stefan-Boltzmann law with observed values for T_{eff} and L_* to determine R_* for G2 and they find an inclination angle to the line of sight of 67° . [J. Bouvier et al. \(1995\)](#) similarly suggest an inclination angle of 50° . None of these studies list uncertainties, but they must be considerable, especially for a peculiar star as G2, as discussed in Section 6.3. We here assume an inclination of 60° , consistent with the above rough estimates, but mainly chosen because at that angle the probability to be higher or lower is equal. For this value the $v \sin i \sim 130 \text{ km s}^{-1}$ corresponds to a true equatorial rotational velocity of $\sim 150 \text{ km s}^{-1}$ and a true radius R_e of $3.6 R_{\odot}$. This is unusually large, for comparison only three stars of the ~ 400 T Tauri stars studied by [L.M. Rebull et al. \(2002\)](#) have comparable or larger radii.

The breakup speed of a star is the Keplerian velocity at the stellar surface $(GM/R_e)^{1/2}$, where M is the stellar mass, G the gravitational constant, and R_e is the stellar radius at the equator (e.g., [A. Maeder 2009](#)). The Roche model for rapidly rotating stars assumes rigid rotation and mass concentrated at the center of the star, and is valid for flattenings (equatorial to polar radius) up to about 1.5. With an equatorial velocity v of 150 km s^{-1} and an equatorial radius r of $3.6 R_{\odot}$ G2 would break up at a rotational velocity of $\sim 180 \text{ km s}^{-1}$ for a mass of $\sim 0.7 M_{\odot}$ suggested by momentum conservation of the two walkaway stars (see the arguments for choosing this mass in Section 6.1). If so, G2 would be rotating at roughly 80% of its breakup velocity, and consequently it would be oblate, with a flattening of roughly 1.3 (Figure 12). This indicates that G2 would appear significantly flattened, almost as much as the extreme case of the fast rotating B3V star Achernar (~ 1.35) ([A. Domiciano de Souza et al. 2014](#)). If G2 has a companion then the companion mass would have to be subtracted, implying that G2 would be less massive and therefore even more oblate. This estimate of the flattening of G2 also depends on the uncertain value of the inclination,

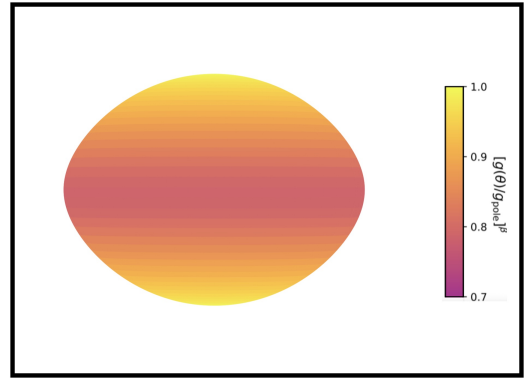


Figure 12. A figure illustrating the oblate shape of G2 with gravity darkening. The flattening (R_{eq}/R_{pol}) is ~ 1.3 , assuming that the mass is $0.7 M_{\odot}$, $r \sin i = 3.1 R_{\odot}$, $v \sin i = 130 \text{ km s}^{-1}$, and $i = 60^\circ$. The gravity darkening exponent is $\beta = 0.16$, as derived by [F. Espinosa-Lara & M. Rieutord \(2011\)](#). The mass and inclination are the most uncertain parameters. For these parameters $\log g_{pole} = 3.40$ and $\log g_{eq} = 2.75$. This can be compared to the (uncertain) measurement of $g \sim 3.6$ (see Section 6.3).

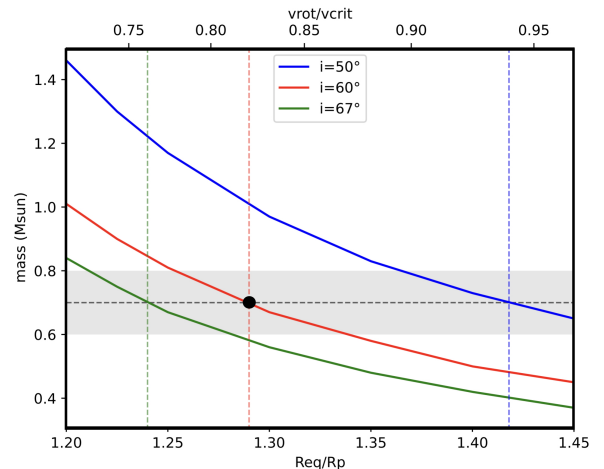


Figure 13. Application of the rigid rotator model to the star HP Tau/G2, showing stellar mass (M) as a function of the rotation rate. The model incorporates observational constraints: projected rotational velocity $v \sin i \approx 130 \text{ km/s}$, and projected equatorial radius $R \sin i \approx 3.1 R_{\odot}$. The plotted curves correspond to stellar inclinations (i): 50° (blue), 60° (red), and 67° (green). Within an assumed mass range of $0.6-0.8 M_{\odot}$, the star is identified as a fast rotator, with its rotation speed constrained between 0.76 and 0.94 of the break-up velocity, depending on the assumed inclination.

see Figure 13 for the range of inclinations suggested by observations. One consequence of the oblate shape of G2 is that gravity darkening takes place around the equator regions, which is discussed in Section 6.3.

6.3. Effective Temperature of G2

From our high resolution K-band spectrum of G2 it is in principle possible to derive or constrain the temperature, $v\sin i$, gravity, magnetic field, and veiling, see C. Flores et al. (2019, 2020, 2022). Using synthetic models, we fit eight wavelength regions containing more than 20 atomic and molecular lines, including Ti, Al, Na, Ca, Fe, Sc, and CO lines,

We derive a K-band temperature of 4200 K, a $v\sin i$ of ~ 130 km s $^{-1}$, and an IR veiling of 0.4. We also derive a gravity $\log(g) \sim 3.6$ and a magnetic field strength of < 1 kG, but due to the extreme width of the lines, we consider the values of gravity and magnetic field to be unreliable. We are confident, however, in the derived temperature values, which are primarily based on the line depth ratios of the more than 20 lines analyzed in the stellar spectrum. We have previously tested the temperature accuracy against selected dwarf, giant, and sub-giant sources with precisely derived temperatures, obtaining median temperature differences of ~ 50 K and standard deviations of ~ 100 K (see Appendix of C. Flores et al. 2019).

C. Flores et al. (2022) studied the effect of star spots on the determination of stellar temperature, and found major differences between those derived from optical and infrared spectra. While the K-band temperature we derive for G2 is about 4200 K, the optical temperature is around 5700 K (G.J. Herczeg & L.A. Hillenbrand 2014). This is the largest discrepancy between optical and infrared temperatures found for any of the young stars studied in C. Flores et al. (2022). We have used a simple two-component model with a hot component, a cold component, and a geometrical filling factor to determine which combinations of these three parameters can reproduce the observed optical (0.5 μ m) temperature of ~ 5700 K (G.J. Herczeg & L.A. Hillenbrand 2014) and K-band T_{K-band} temperature of 4200 K. In this two-component model, we assume that: (a) the cold and hot components are represented by Planck functions $B(T)$; (b) the filling factor is a geometrical filling factor; and (c) at each wavelength, the observed temperature is the weighted average of the hot and cold temperatures, see equations C1 to C3 in C. Flores et al. (2020). We find that there is a large family of solutions for the specific cold and hot temperature components that satisfy both spectroscopic observations, with assumed temperature uncertainties of 150 K. However, a minimum filling factor of 70% is required, with even larger filling factors also possible, to satisfy these conditions. This demonstrates that if the surface of G2 is indeed mainly characterized by two temperatures, then surface spots covering a significant fraction of the stellar area are unavoidable.

In principle we could instead determine T_{eff} from the luminosity and radius of the star. But this assumes that the star is spherical, and we have shown that G2 must have an oblate shape. As such it is affected by gravity darkening, which occurs because the centrifugal acceleration at the equator offsets the star's gravity. H. von Zeipel (1924) showed that the effective temperature for fast rotating radiative stars are a function of latitude, with $T_{eff} \propto g^\beta$, where g is the local gravity, and β is the gravity-darkening exponent. Modifications to β are required for convective stars such as G2 (e.g., Lucy 1967; C. Claret 2012).

It follows that both spots and gravity darkening affect G2, and that determinations of effective temperature for a star like G2 should be treated with caution.

7. DISCUSSION

In the preceding pages we identified G2 as a highly unusual star, and showed that G2 and KPNO 15 are walkaway stars moving apart following a dynamical dissociation of a young triple system about 5600 yr ago. In the following we discuss the dynamics of such small multiple systems.

7.1. The Dynamical Evolution of Multiple Systems

Non-hierarchical multiple systems are inherently unstable, and their decay is a stochastic process, which occurs on a time scale of ~ 100 crossing times (e.g., J.P. Anosova 1986), for a recent review on triple systems see H.B. Perets (2026). This most often happens in the embedded protostellar phase (e.g., B. Reipurth et al. 2010). The end result, after a period of cgaotica motions, is either a multiple system with a hierarchical structure or the system breaks apart.

As a result, the remaining system becomes increasingly eccentric, statistically following a thermal distribution, and hence the ultimate bound binary often possesses a very high eccentricity. During protostellar evolution when the stars are surrounded by circumstellar and ambient material, periastron passages can lead to dissipative disk interactions that eventually cause the binary orbit to shrink. Close binaries (less than ~ 10 AU) are not formed in the collapse of a cloud core, so such dynamical evolution explains the existence of spectroscopic binaries among young stars. In some more extreme cases, the end result can be a merger of the two components (e.g., K. Rawiraswattana et al. 2012; S. Toonen et al. 2022). C. Shariat et al. (2023) estimate that at least 30% of solar-type stars were formed in hierarchical triples.

Non-hierarchical triple systems are inherently unstable, and one component, often the least massive, can be

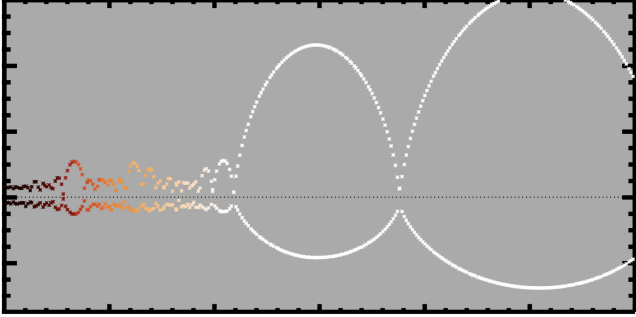


Figure 14. Non-hierarchical triple systems are unstable, and will eject one component typically after about 100 crossing times (M. Valtonen & S. Mikkola 1991). However, while the ejected body in some cases can escape, it is more common that it is ejected into a bound orbit. This may be a stable orbit, or it may return to trigger another episode of interactions which leads it to be ejected again. This can numerous times before either a stable triple configuration is achieved or the third body escapes. An example of a simulation, shown here for the first 300,000 yr, reveals numerous ejections that all return the third body before it finally escapes (outside the figure) after about 1 million yr (B. Reipurth et al. 2010). The colors indicate extinction from a slowly disappearing cloud core. As the core loses mass, the gravity well weakens, facilitating larger excursions. The dashed line indicates the center of mass of the system.

ejected again and again into a bound orbit before either being ejected into an escape or achieving a stable hierarchical configuration. The ratio of inner to outer separation in the triple system that is required to achieve stability is a complex function of the orbital characteristics, but is roughly of the order of 10. If stability is not achieved, the three components will interact again. Numerical simulations show that this can go on for a long time, up to ten million years, with the third body being repeatedly ejected into bound but unstable orbits. Some ejections can last from a few thousand years to in some cases more than a million years before the third body returns to the remaining binary (B. Reipurth et al. 2010; B. Reipurth & S. Mikkola 2012). As a result, protostars are more often found with a distant companion than more evolved young stars (M.S. Connelley et al. 2008a,b; J. Tobin et al. 2022).

The disruption of a multiple system of N bodies will eventually lead to the existence of at least one stable binary. Depending on the masses of the components, the energies involved in the disruptions, and the amount of circumstellar material that can alter the binary orbit, the resulting binary can have a large range of semimajor axes. In the ultimate case the two components can merge.

7.2. Coalescence

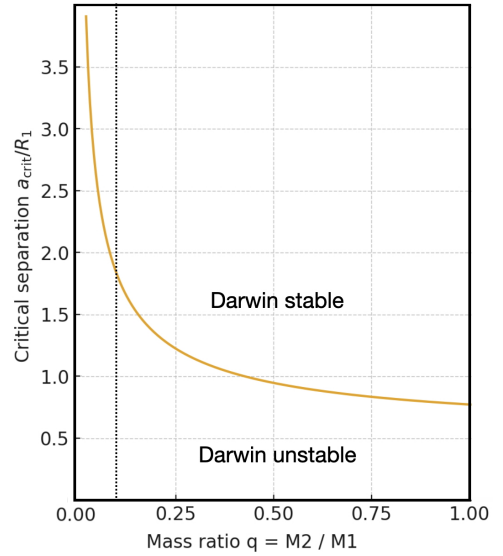


Figure 15. The limit between Darwin stable and Darwin unstable binaries is a steep function of the mass ratio. Very small mass ratios < 0.1 are far more likely to lead to a merger than binaries with higher mass ratios. R_1 is the radius of the primary and a_{crit} is the separation at which the binary becomes Darwin unstable.

Two stars can coalesce either via collisions or via mergers. The former may occur in environments with extreme stellar densities and are unpredictable, whereas the latter may occur in binary systems which in various ways are losing angular momentum and spiral in. For a comprehensive review, see F.R.N. Schneider (2025).

When binary systems evolve they can in some cases reach the point where the Darwin instability is triggered (G.H. Darwin 1879; P. Hut 1981; K. Stepień 2011; J.L.A. Nandez et al. 2014). In a binary that has become Darwin-unstable, tides try to spin up the primary star at the expense of orbital angular momentum, but the spin of the orbit changes faster than the spin of the primary, so synchronization is never achieved. More specifically the Darwin instability limit is crossed when the orbital angular momentum J_{orb} is less than three times the spin angular momenta of the two stars, i.e. $J_{orb} < 3(J_{spin1} + J_{spin2})$. As orbital angular momentum continues to be removed, the orbit shrinks, and the primary spins up. Eventually the stars may reach contact and the stars will merge on an orbital time scale. This can happen for a variety of reasons, for example if stellar evolution leads one component to expand, or if the Kozai-Lidov mechanism shrinks the binary orbit. J. Henneco et al. (2024) identify five pathways that can lead to contact and mergers. Mergers are more likely to happen if the secondary is much smaller than the primary (Figure 15).

Coalescence of two stars is not uncommon at late evolutionary stages (e.g., C.S. Kochanek et al. 2014). Blue straggler stars are regularly found in globular and open clusters, and are in many cases well interpreted as the result of collisions between two cluster members (e.g., J.G. Hills & C.A. Day 1976). N.W.C. Leigh et al. (2017, 2018) have studied collision probabilities in small N-body systems and demonstrate that the probability rises as N^2 . H.B. Peters & D.C. Fabrycky (2009) and S. Naoz & D.C. Fabrycky (2014) have proposed that blue stragglers may instead originate in hierarchical triple systems in which the inner binaries evolve into close binaries or contact binaries by a combination of Kozai-Lidov cycles leading to increasing eccentricity and then tidal friction which will lead to orbital circularisation (e.g., P. Eggleton & L. Kiseleva-Eggleton 2001). Mass transfer in such close binaries could then lead to merger events. New simulations of three-body dynamics show that this may be a common phenomenon (C. Shariat et al. 2025).

The modelling of stellar mergers has a long history (e.g., F.G.P. Seidl & A.G.W. Cameron 1972; W. Benz & J.G. Hills 1987; N. Soker & R. Tyrenda 2006). Recent three-dimensional magnetohydrodynamic simulations of massive stars have resulted in a detailed understanding of the merging process (F.R.N. Schneider et al. 2019). During a thermal relaxation phase after the coalescence, the merger product reaches critical surface rotation and begins to shed mass. The merger product can only lose angular momentum through mass loss (from stellar winds or from shedding mass when the star rotates critically) and from magnetic braking. Eventually the internal structure of the merger product adjusts and subsequently it evolves as a normal single star of the combined mass.

An important characteristic of coalesced stars is their strong magnetic fields, which result because turbulent mixing greatly amplifies magnetic field energies (L. Ferrario et al. 2009; D.T. Wickramasinghe et al. 2014; F.R.N. Schneider et al. 2020).

Young stars are subject to the same processes as evolved stars, but in addition the association with molecular clouds and the presence of massive circumstellar and circumbinary disks can play additional important roles for the dynamical evolution of newborn binaries and multiples. Binaries closer than roughly 10 AU cannot be formed by fragmentation, but both mass accretion (e.g., M.R. Bate et al. 2002) and dynamical friction (e.g., S.W. Stahler 2010) play important and efficient roles in the orbital evolution of newborn multiple systems. A.T. Lee et al. (2019) have carried out 3D magnetohydrodynamic simulations of turbulent star

forming clouds, and find that such evolution can occur on time scales as short as ~ 0.1 Myr or less. For an up-to-date review of the literature on newborn multiples, see S.S.R. Offner et al. (2023). In short, conditions are commonly available that can facilitate the merger of young stars.

Observationally, numerous studies exist, and especially two events have provided important empirical information on mergers: the eruption of V838 Mon in 2002, and the eruption of V1309 Sco in 2008, see Appendix D.

7.3. What can we learn from late stellar evolution?

It is tempting to ask what similarities there may be between mergers among pre-main sequence stars and among evolved stars.

Binaries that have evolved past the main sequence are involved in a plethora of high energy stellar phenomena divided into many classes of stars and displaying an almost bewildering variety of spectral signatures and types of variability. Young stars and evolved stars are different in very many ways, so in the following we will merely examine certain stars in late stellar evolution that may act as a broad guide to understand the peculiarities of G2.

7.3.1. W UMa stars and the formation of contact binaries

W UMa stars are low-mass eclipsing contact binaries that touch each other at the L1 Lagrangian point and share a common envelope. They generally have spectral types from late A to mid K and have stellar activity which likely derives from a coupling of convective motions with fast rotation that drives a dynamo. They have periodic light curves, typically with periods shorter than 1 day, but there may be a tail to 1.3-1.5 days. Most contact binaries are observed to be part of triple or higher order multiple systems (e.g., A. Tokovinin et al. 2006; S.M. Rucinski et al. 2007).

7.3.2. FK Com stars

Some W UMa binaries will merge during their common envelope evolution and become single fast-rotating stars (e.g., J. Hennec et al. 2024). It is generally assumed that such newly single stars emerge as FK Com stars. This is a small group of peculiar stars identified by B.W. Bopp & S.M. Rucinski (1981) and B.W. Bopp & R.E. Stencel (1981). Not many of these stars are known, possibly indicating that they are in a relatively shortlived evolutionary phase. The prototype FK Com is a high-probability runaway star with a velocity of ~ 33 km s $^{-1}$ (N. Tetzlaff et al. 2011), a spectral type of G4III

Table 3. Comparison of HP Tau/G2 with HD 283572 and FK Com

Parameter	HP Tau/G2	Ref. ^a	HD 283572	Ref. ^a	FK Com	Ref. ^a
SpT	G2	H14	G5IVe	W87	G4III	S09
H α emiss.	weak	C79	no	S94	weak	R81, W93
Lithium	yes	***	yes	W87,P93	no	
Distance	162.2/0.9 pc	T09	128.5/0.6 pc	T07	224.7/1.5 pc	G22
Low-ampl. var.	yes (V1025 Tau)	V89	yes (V987 Tau)	G08	yes (FK Com)	S23
Period	1.2 days	V89	1.5 days	W87,G08	2.4 days	J93
$v\sin i$	127 ± 4 km s $^{-1}$	N12	79 - 136 km s $^{-1}$	N12,W87	159 ± 4	R90
$r\sin i$	$3.1 R_{\odot}$	R26	$2.39 \pm 0.03 R_{\odot}$	S98	$7.5 R_{\odot}$	J93
Inclination	$50\text{--}67^{\circ}$	H86,W87,B95	$\sim 35^{\circ} ({}^{+15}_{-5})$	S98	$\sim 60^{\circ}$	K99
Mass	$1.9 \pm 0.2 M_{\odot}$ ^b	T09,M20	$1.8 \pm 0.2 M_{\odot}$ ^b	S98		
L_{bol} ^c	$10.3 L_{\odot}$	R26	$6.4 L_{\odot}$	R26	$23 L_{\odot}$	R26
Age	$3.6\text{--}5.0$ Myr ^d	R20,G24	$2.5\text{--}9$ Myr	L24	$5\text{--}10$ Gyr	G86
Flares	yes	R26	yes	F98	yes	O99
Radio Cont.	non-thermal	B84	thermal	O90	non-thermal	R91
X-rays	yes	G07	yes	W87,S94,F98	yes	D08
Gaia RUWE	3.85	G22	0.93	G22	1.16	G22
Large star spots	yes	R26	yes	J94,S98	yes	K07
Walkaway/Runaway	yes	L18,R26	no	R26	yes	T11

NOTE—(a): B81: B.W. Bopp & S.M. Rucinski (1981); B84: J.H. Bieging et al. (1984); B95: J. Bouvier et al. (1995); C79: M. Cohen & L. Kuhf (1979); D00: G. Duvert et al. (2000); D08: J. Drake et al. (2008); F98: F. Favata et al. (1998); G86: E.F. Guinan & C.R. Robertson (1986); G07: M. Güdel et al. (2007); G08: K.N. Grankin et al. (2008); G22: Gaia DR3; G24: A. Garufi et al. (2024); H14: G.J. Herczeg & L.A. Hillenbrand (2014); H86: W. Herbst (1986); J93: L. Jetsu et al. (1993); J94: I. Joncour (1994); S.J. Kenyon & L. Hartmann (1995); K99: H. Korhonen et al. (1999); K00: H. Korhonen et al. (2000); K07: H. Korhonen et al. (2007) K11: A.L. Kraus et al. (2011); L18: K.L. Luhman (2018); L24: J.B. Lovell et al. (2024); M20: D.J. Mullan & J. MacDonald (2020); N12: D.C. Nguyen et al. (2012); O90: D. O’Neal et al. (1990); O99: J.M. Oliveira & B.H. Foing (1999) P93: R.J. Patterer et al. (1993) R81: L.W. Ramsey et al. (1981); R15: J.L. Rivera et al. (2015); R20: A.C. Rizzuto et al. (2020); R26: this paper; R90: S.M. Rucinski (1990); R91: S.M. Rucinski (1991); S94: K.M. Strom & S.E. Strom (1994); S98: K.G. Strassmeier & Rice (1998); S09: K.G. Strassmeier (2009); S11: M. Siwak et al. (2011); S23: I.S. Savanov et al. (2023); T07: R.M. Torres et al. (2007); T09: R.M. Torres et al. (2009); T11: N. Tetzlaff et al. (2011); V89: F.J. Vrba et al. (1989); W87: F.M. Walter et al. (1987); W93: A.D. Welty et al. (1993); W96: S.J. Wolk & F.M. Walter (1996).

(b): Masses from evolutionary tracks assuming normal stars. We argue that these masses are wrong, and that the mass of G2 is much smaller, $\sim 0.7 M_{\odot}$, based on conservation of momentum considerations.

(c): Luminosities were calculated by integrating under the optical/infrared photometry. For G2 an $A_V = 2.55$ was adopted (HH14), for HD 283572 an $A_V = 0.75$ was used (SS94), and for FK Com no extinction was assumed.

(d) Age determined from evolutionary models assuming a normal star. In reality G2 is likely to have the same age as the surrounding group, $\sim 2.0 \pm 0.3$ Myr, see Section 3.

(K.G. Strassmeier 2009), and a spectrum showing a weak and variable H α emission line (e.g., L.W. Ramsey et al. 1981; A.D. Welty et al. 1993), see Appendix E. Ca II H and K lines are in emission, indicating chromospheric activity (e.g., K. Vida et al. 2015). The star rotates very rapidly, with a $v\sin i$ around 160 km s $^{-1}$ (e.g., S.M. Rucinski 1990) and its rotational period is 2.4 days (L. Jetsu et al. 1993), which implies a radius $r\sin i$ of $7.5 R_{\odot}$. D. Huenemoerder et al. (1993) argue that the star is rotating near its breakup velocity. A.D.

Welty & L.W. Ramsey (1994a) interpret a series of H α profiles (width ~ 1000 km s $^{-1}$) as evidence for nonradial pulsations which they postulate is evidence for a recent merger. On longer timescales the star shows irregular low-amplitude variability (e.g., K. Panov & D. Dimitrov 2007). The variability is ascribed to giant star spots, which have been observed with Doppler imaging that shows spots preferentially located at high latitudes (H. Korhonen et al. 2000, 2007). These are an indication of strong magnetic fields (H. Korhonen et al. 2009).

FK Com is an active X-ray source (e.g., [A.D. Welty & L.W. Ramsey 1994b](#); [J. Drake et al. 2008](#)) and has been studied at ultraviolet wavelengths by [T.R. Ayres et al. \(2016\)](#). Non-thermal radiation in the 3.6 cm radio continuum has also been detected ([S.M. Rucinski 1991](#)). [E.F. Guinan & C.R. Robertson \(1986\)](#) conclude that it is a member of the old disk population, with an inferred age around $5\text{--}10 \times 10^9$ yr.

Table 3 gives a detailed comparison between G2 and FK Com itself. Remarkably, we find that they have almost identical properties. At first glance it is puzzling that two stars can be so similar considering their very different evolutionary stages.

Once two stars have merged, they lose their identity and for a while the new star is instead dominated by the aftermath of the merger as it evolves on a thermal time scale towards an undisturbed star with the characteristics of a more massive star. Hence, a merger of either two young stars or of two evolved stars will for a while look if not identical then very similar.

A star newly formed in a merger will at least initially be rotating very fast, but the star will eventually (and sometimes even rather quickly) spin down and become a slow rotator. This can be due to internal structure changes that lead to a re-distribution of angular momentum, or from mass loss (magnetized winds, outflows, or equatorial decretion disks) that will carry a significant amount of angular momentum away ([T. Ryu et al. 2025](#)).

We suggest that the merger of two young stars will result in a bloated star like the FK Com stars, and that G2 may be such a case.

Neither G2 nor FK Com are similar to the post-eruption appearance of the evolved star V1309 Sco (see Appendix D), which immediately after the eruption had an F-type spectrum that turned into a red giant spectrum within a month. However, V1309 Sco erupted less than 20 years ago, while the G2 merger most likely happened several thousand years ago. During that time-span, if a cool dusty envelope was ejected in the eruption, it would have dispersed.

7.4. G2 as a Merger

If G2 is a merger, an immediate question is why this happened now, ~ 2 Myr after the group formed, when there is very little dissipative material left in the system. Such a viscous environment would be essential to make two components spiral in and merge.

It is evidently not possible now to reconstruct the precise dynamical evolution of a chaotic system that led to the current state of G2 and the other walkaway stars in

the group. But in the following we hazard a guess to what *might* have taken place.

The group of 12 stars and brown dwarfs around HP Tau is one of the most compact and rich groupings in Taurus ([I. Joncour et al. 2018](#)), yet is about 2 Myr old ([D.M. Krokowski et al. 2021](#)). If we assume that the individual stars in the central group have space velocities of ~ 1 km s $^{-1}$, and if we take the angular separation between G2 and FF Tau as the size of the multiple system in the plane of the sky (radius 7.3 arcmin at 162 pc, see Figure 2), then it should take of the order of 400,000 years to spread beyond this volume. But the age of the system is about 5 times larger. This suggests that the group may have remained tenously bound until more recently, probably because the cloud core that gave rise to the stars survived for a long time,

A high order multiple system of at least 6 bodies then remained, consisting of G2 (at the time a binary, and possibly a compact triple if the Gaia companion is real), G3 (a binary), and the two late M-dwarfs KPNO15 and G1. In order to stay bound together, even loosely, this multiple system had to be hierarchical, consisting of two separate groups (the G2 binary plus KPNO 15, and the G3 binary plus G1) tenuously bound together.

As noted in Section 7.1 such systems are generally born unstable and typically become hierarchical by ejecting a component (either bound or unbound) already within about 100 crossing times, which in most cases occurs during the protostellar stage. But the resulting hierarchical configuration is not necessarily stable, so upon return, an ejected body may be sent away again and again (Figure 14). This process can sometimes go on for a very long time, numerical simulations show that up to 10 million years or even more can pass before the ejected star, after numerous excursions, is finally either escaping or parked in a stable eccentric orbit ([B. Reipurth et al. 2010](#); [B. Reipurth & S. Mikkola 2015](#); [S. Toonen et al. 2022](#)). KPNO 15 and G1 must have undergone such extensive 'yo-yo' episodes over the past ~ 2 million years.

At some point, maybe 6000 years ago, this fragile little aggregate somehow became disturbed, perhaps by the nearby more massive binary HP Tau. Whatever the disturbance was, the G2+KPNO15 and the G3+G1 multiple systems each broke up roughly at the same time (~ 5600 yr and ~ 4900 yr, respectively) forming two slowly separating walkaway pairs (Fig 16).

In the case of G2, the ejection of KPNO 15 into an escape was the final step in the cascade that had bound the components of the G2 binary ever tighter in a highly eccentric orbit, and rather than resulting in a tight spec-

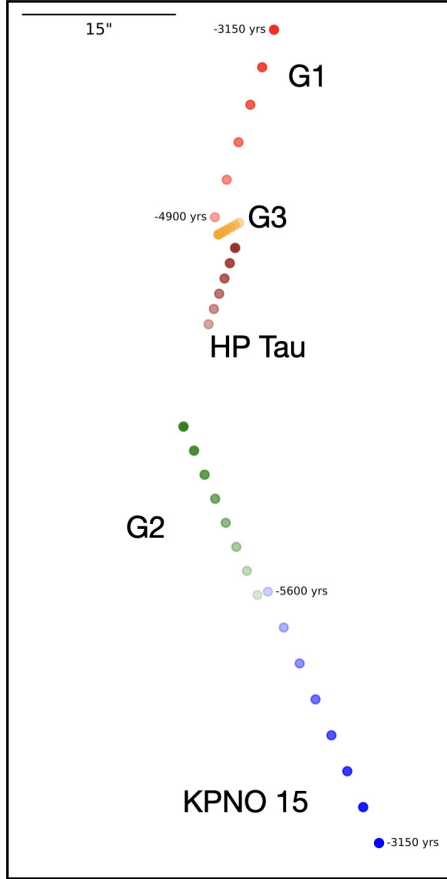


Figure 16. The motions of G1, G2, G3, KPNO 15 and HP Tau are shown in this figure in the time interval from 5600 to 3150 yr ago in steps of 350 years. The nominal time of breakup for the G2/KPNO 15 pair is 5606 yr and 4869 yr for G1/G3. Note that the position and proper motion of G3 is affected by its close (31 mas) companion. The K4 star HP Tau is slowly crossing the stellar group and possibly disturbing it. It has an unusually high velocity, although not high enough to be labeled a walkaway star.

troscopic binary as G3, in this case the binary became Darwin unstable and merged.

A few details of the process can be extracted. If KPNO 15 has a mass of $\sim 0.4\text{--}0.5 M_{\odot}$ then the G2 precursors (plus the putative Gaia companion) would have a total mass of roughly $\sim 0.7 M_{\odot}$, indicating that the components would have been very low mass stars or brown dwarfs. That KPNO 15 is a walkaway star and not a runaway star indicates that the dynamical interaction triggering the ejection was not a particularly close one, with separations not much closer than ~ 10 AU.

The above broadly outlined scenario is of course very speculative, but the general dynamical process is well understood, and in fact is probably an integral part of how parts of dense clusters dissolve.

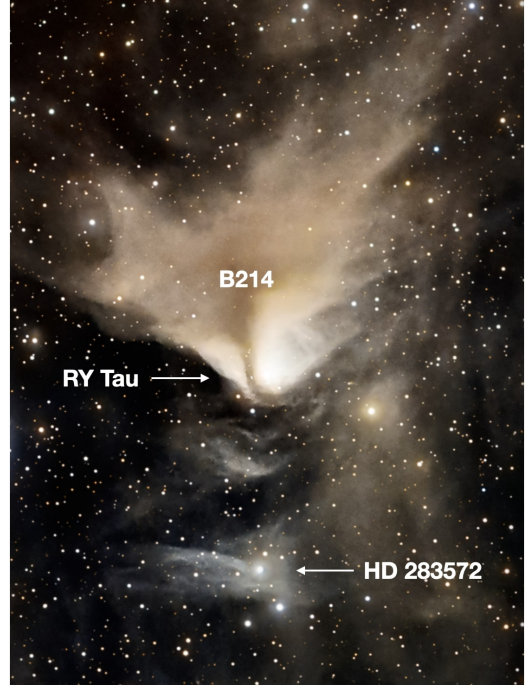


Figure 17. HD 283572 is located near the little cloud B214, close to RY Tau which illuminates the LBN 785 = vdB27 reflection nebula. Note that the well defined cometary shape of the B214 cloud points straight towards HD 283572. No other such cometary clouds are seen in this region of Taurus. Courtesy Cédric Mauro and Christophe Marsaud from Team Astrofleet.

It is possible that more accurate data from future Gaia releases may provide a fuller understanding of a possible relation between these three walkaway stars.

7.5. Are there other cases like G2?

G2 is a highly unusual star, and we believe that it is best understood as the result of a merger. If so, could similar characteristics in other young stars suggest recent mergers? We are aware of only one star that shares almost all important features with G2, and it is HD 283572 (V987 Tau) near the small Barnard 214 cloud in Taurus. It is part of an aggregate of ~ 35 YSOs near L1495E (K.M. Strom & S.E. Strom 1994). R.M. Torres et al. (2007) used VLBA to determine a distance of 128.5 pc and Gaia DR3 gives 127.0 pc. HD 283572 was initially recognized as a young X-ray source by E. Feigelson & J. Kriss (1981) and F.M. Walter & L.V. Kuhi (1981). Subsequently F.M. Walter et al. (1987) carried out a detailed study and classified HD 283572 as a G5IV star with lithium and a fast rotational period P of 1.54 days (K.G. Strassmeier & Rice 1998), which we confirmed with TESS data. It has no infrared excess out to $60\ \mu\text{m}$ (S.J. Wolk & F.M. Walter 1996; K.G. Stassun et al. 2001). It is a weak-line TTS with variable H α

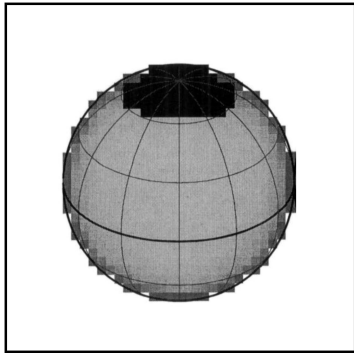


Figure 18. A photospheric temperature map of HD 283572 from I. Joncour (1994) obtained with Doppler imaging and showing a large polar spot. The maximum temperature difference is 1600 K.

profile and signs of chromospheric activity (M. Fernandez & L. Miranda 1998). The star is a fast rotator with a $v\sin i$ of 79.5 ± 3.0 km s $^{-1}$ (C.M. Johns-Krull 1996), and confirmed by J.-F. Donati et al. (1997) [77 km s $^{-1}$] and K.G. Strassmeier & Rice (1998) [78 \pm 1 km s $^{-1}$]. An extreme millimeter flare was detected by J.B. Lovell et al. (2024).

I. Joncour (1994) have presented Doppler imaging of the star and discovered a large polar spot (Figure 18), which was confirmed by K.G. Strassmeier & Rice (1998), who found the polar spot to be one of the largest and coolest ever observed, with at most few spots at lower latitudes.

M. Siwak et al. (2011) obtained a detailed light curve of HD 283572 which shows characteristic low-amplitude fluctuations ascribed to spots. C.L. Davies et al. (2014) suggest a mass of $1.98^{+0.19}_{-0.25} M_{\odot}$, a radius of $2.84 R_{\odot}$, and an age of $5^{+2.6}_{-1.2}$ Myr based on evolutionary tracks. As is the case for G2, we suspect that these values are much too high.

When P and $v\sin i$ are combined this indicates a $r\sin i$ of $2.4 R_{\odot}$, which for an inclination of roughly 35° (K.G. Strassmeier & Rice 1998) suggests a large equatorial radius of $\sim 4.1 R_{\odot}$. If the mass of HD 283572 would be the same ($\sim 0.7 M_{\odot}$) as for G2, then it would have about the same oblate shape as G2, with a flattening (R_{eq}/R_{pol}) of roughly 1.4.

If HD 283572 is a recent merger, then a major eruption must have taken place. The star, however, is not directly associated with a dense cloud, only some wisps of nebulosity, so no surrounding shell has been formed as in the case of G2. But to the north there is a small cloud, B214, which has a striking cometary appearance, with a symmetry axis pointing straight towards HD 283572. No other cometary clouds are seen in this part of Tau-

rus. We speculate that the unusual shape of the B214 cloud is due to an energetic event in HD 283572.

There are several other potential cases, for example HD 30171 (e.g., R. Wichmann et al. 2000). It should be emphasized that it is the combination of the various peculiarities that indicate a possible merger, not just the G spectral type. There are many normal young G-stars that are on their way to become Herbig Ae/Be stars and which have nothing to do with mergers.

The Gaia DR3 proper motions of HD 283572 is almost identical to the mean of all YSOs closer than 3 arcmin. Its heliocentric radial velocity is $+14.2$ km s $^{-1}$ (J.L. Rivera et al. 2015), that is, within ~ 5 km s $^{-1}$ of the cloud velocity. Hence HD 283572 is not a walkaway star. We have searched the Gaia DR3 catalog for any star moving directly away from HD 283572, but none were found.

The features of HD 283572 may suggest that it has suffered a past merging event, when the star was no longer associated with a substantial molecular cloud core, therefore probably at a slightly later stage than G2. If so, it may indicate that G2 is not a pathological case, but represents a not uncommon phenomenon, albeit infrequent on human time-scales.

7.6. When did the merger take place?

The accurate Gaia proper motions indicate that the triple disintegration event that produced the walkaway stars G2 and KPNO 15 took place ~ 5600 yr ago. In principle, the ensuing merger event could have taken place at any time after that. For lack of better constraints we speculate that the explosion might have taken place when G2 was at the center of the bright innermost part of the reflection nebula, marked by the orange circle in Figure 3. If so, then it occurred roughly 2000 yr ago.

7.7. The Past and Future Evolution of G2

In Section 6.1 we referred to the derivation of model isochronal ages and masses for G2 by A.C. Rizzuto et al. (2020), D.J. Mullan & J. MacDonald (2020) and A. Garufi et al. (2024), who found ages in the range 3.6-5.0 Myr, significantly higher than the derived age of 2.0 ± 0.3 Myr for the neighboring stars in the little T Tauri group. The derived mass of $\sim 2 M_{\odot}$ is also inconsistent with the mass derived from analysis of the Gaia proper motions of G2 and KPNO 15.

In light of the merger hypothesis, these discrepancies find a natural explanation when G2 is seen as the bloated merger of two low-mass late-type young stars. When the eruption took place G2 reached a much higher luminosity and an earlier spectral type. As a result, G2 moved

upwards and to the left in the HR-diagram, to evolutionary tracks for much more luminous and warm stars with higher masses.

The evolution of mergers can be divided into three phases with different timescales. The first is the period following the ejection of the third star during which the newly contracted binary begins a series of dissipative periastron passages. This can be long or short depending on the orbital characteristics and the amount of circumstellar gas. But once the two stars are in contact, the second phase of actual coalescence and eruption is brief. This is consistent with observations of V1309 Sco, which erupted and declined to close to its pre-outburst brightness within about 3 years (R. Tylenda et al. 2011). However, the resulting star is still out of thermal equilibrium, so during a third phase it will evolve towards a stable configuration corresponding to the new higher mass. This will be achieved on a Kelvin-Helmholtz timescale

$$t_{KH} \approx \frac{GM^2}{RL}$$

where G is the gravitational constant, and M , R , and L are the mass, radius, and luminosity of the merger remnant.

For an assumed mass for G2 of $\sim 0.7 M_{\odot}$ from momentum conservation with the KPNO 15 walkaway star, and an estimated radius (assuming an inclination of $\sim 60^\circ$) of $3.6 R_{\odot}$, and an assumed peak luminosity of $1000 L_{\odot}$ we find a Kelvin-Helmholtz time of ~ 4000 yr. Given the assumptions this number is obviously uncertain, but it indicates that the star may have observable peculiarities for several thousand years, consistent with the upper limit of 5600 yr for the time of the merger. For details on the post-merger evolution from 3D MHD simulations, see F.R.N. Schneider et al. (2020).

The effect of accretion on the luminosity and evolution of low-mass stars and brown dwarfs has been explored by a number of authors, e.g., E.I. Vorobyov et al. (2017), S.S. Jensen & T. Haugbølle (2018), and V. Elbakyan et al. (2019). In the latter paper, the episodic excursions that low-mass protostars take in the HR-diagram are compared with observations of FUor eruptions. Figure 19 is from the V. Elbakyan et al. (2019) paper, and shows the current location of a number of FUor eruptions (black diamonds) in a theoretical HR diagram. We have inserted the current positions of G2 and HD 283572. They have luminosities that are roughly similar to what would be expected from young stars with their optical spectral types, so they have had time to decline from their peak brightness.

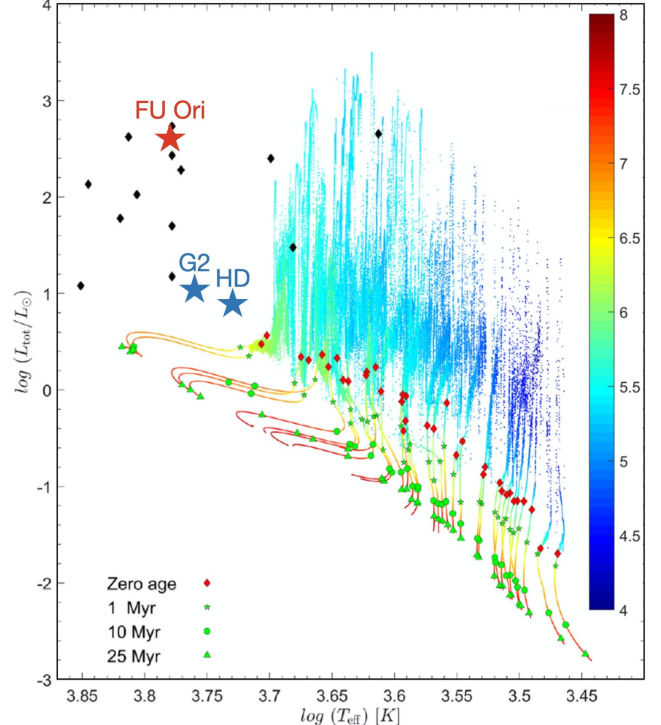


Figure 19. The location of a number of FUors (black diamonds) compared with evolutionary tracks and models at a range of ages (ages of models are indicated in the bar) in a figure adapted from Figure 9 of V. Elbakyan et al. (2019), see their paper for further details. The current location of G2 and HD 283572 are plotted, with temperatures adopted from their optical spectral types. Eruptions in low-mass stars allow them to appear more massive and warmer than their actual masses would indicate. We argue that G2 and HD 283572 after their merger events occupied positions further up to the left and as they are now undergoing restructuring they gradually move towards the location of quiescent stars corresponding to their new increased masses.

At the time of the mergers, G2 and HD 283572 would have been significantly more luminous than now, and it is possible that, if they at the time had been observed, they might have been classified as FUors.

In Appendix F we speculate about the relation between mergers and FUor eruptions.

8. THE REFLECTION NEBULA

Our multi-filter APO observations show that the HP Tau system is surrounded by a pure reflection nebula, without any shocked emission. As shown in Figure 1, the reflection nebula consists of a nested set of partial shells roughly centered on the compact group of stars consisting of HP Tau, G2, and G3 (Figure 1). The brightest emission arises from a corrugated partial arc of emission which wraps around these three stars and opens-up towards the south and which we call the

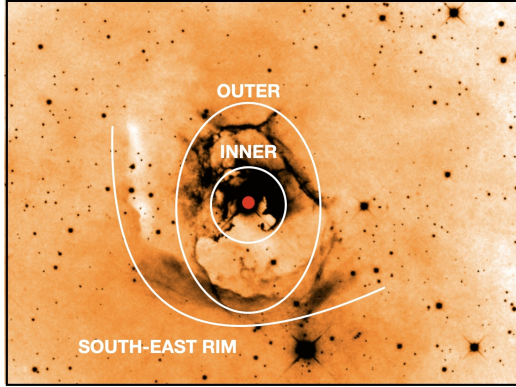


Figure 20. An optical image of the Magakian 77 reflection nebula with the three main rims identified. The red dot marks the position of G2. Image courtesy Adam Block.

inner rim or inner shell (see Figure 20). A protrusion located about $12''$ north of G2 exhibits the highest surface brightness. A sub-cavity with a radius of about $14''$ forms an indentation centered on HP Tau. This inner nebula is surrounded by a dimmer, elongated shell with a radius of $\sim 100''$ from HP Tau towards the north and $\sim 200''$ towards the south. This shell has a width ranging from 90 to $130''$ in the east-west direction and appears to open, or simply be much dimmer, towards the south. In the following, we refer to this as the outer rim. While the northwest section of the outer rim forms a well defined straight wall, its northeast portion is filamentary and highly structured. Several sub-cavities are seen throughout the nebula. The walkaway star G1 is located in the northern part of the inner shell and is slightly nebulous, indicating its association with the cloud. The walkaway star KPNO 15 is centered in what appears to be an evacuated lobe. Finally, a clam-shell shaped, partial outer rim envelops the entire group of young stars, here labeled the south-east rim.

The narrow-band H α , [S II], and H $_2$ images failed to reveal any emission line nebulosity which would have indicated the possible presence of shocks or fluorescent emission from UV-irradiated cloud edges. Thus, the HP Tau system does not currently power Herbig-Haro objects or molecular hydrogen objects above our sensitivity limit.

9. MILLIMETER OBSERVATIONS

9.1. Low Velocity ^{12}CO Streamers from G2

The HP Tau region has attracted surprisingly few mm studies despite the concentration of young stars. [G.H. Moriarty-Schieven et al. \(1992\)](#) made a single ^{12}CO ($J=3-2$) pointing towards HP Tau, and concluded that there is blue- and red-shifted emission in the region.

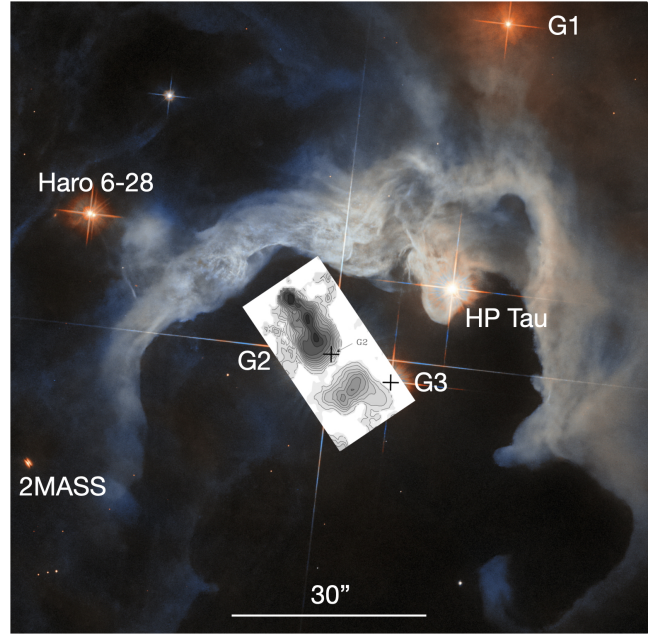


Figure 21. The reflection nebula around G2 as seen with HST through several broadband filters (Credit G. Dûchene & G. Kober/ESA). Overlaid is the ^{12}CO ($J=2-1$) interferometric observations by [G. Duvert et al. \(2000\)](#) showing the small bipolar outflow emanating from G2 that they discovered with a total extent of about 5,000 AU. The two crosses represent G2 and G3. The main YSOs are identified. 2MASS refers to J04355760+2253574, which displays an edge-on disk shadow (see Figure 26).

[G. Duvert et al. \(2000\)](#) used the IRAM Plateau de Bure interferometer to observe the ^{12}CO ($J=2-1$) line towards G2 with a $3''$ beam. They found a compact, very low-velocity entirely redshifted flow with a well defined, $>10''$ -long (>1600 AU) lobe emanating from G2 towards position angle $\sim 25^\circ$. The radial velocity ranges from $V_{LSR} = 8.2 \text{ km s}^{-1}$ near the star to 10.2 km s^{-1} at the northeast end of the lobe. In the counterflow direction, there is a $\sim 5''$ -long (~ 800 AU) patch which is also redshifted with $V_{LSR} = 10.5 \text{ km s}^{-1}$ (Figure 21). Thus, this feature only exhibits redshifted emission and is not bipolar.

Furthermore, a bipolar outflow is unexpected for a star apparently with little or no circumstellar material. However, compact bipolar outflows

are a characteristic of some recent stellar mergers ([T. Kamiński et al. 2015, 2020; F.R.N. Schneider et al. 2019, 2020](#)). It is possible that the low-velocity, redshifted only feature may trace tidal streamers launched shortly before or during the stellar merger along the orbit plane defined by the stars that merged to form G2.

The Taurus outflow survey by [G. Narayanan et al \(2012\)](#) using the FCRAO maps of Taurus ([G. Narayanan](#)

et al. 2008) did not find a larger-scale outflow. Subsequently, Li et al. (2015) used the FRCAO data for a deeper survey, and detected blue-shifted emission in the general region of HP Tau, which they interpreted as an outflow (TMO-39). They likely saw the approaching side of the expanding shells (see the following discussion).

Molecular outflows are sometimes associated with optical shocks. C. Aspin & B. Reipurth (2000) obtained [SII] images around HP Tau, but found no such shocks. We obtained deeper images with the APO 3.5-m telescope in H α and [SII] and confirm the absence of Herbig-Haro objects.

9.2. New ^{12}CO and ^{13}CO Data

We obtained ^{12}CO (J=3-2) and ^{13}CO (J=3-2) maps of the gas around the area of the Magakian 77 reflection nebula (Figure 22), see Section 2 for details of the observations.

Figure 22 shows the kinematics of the ^{12}CO emission associated with the HP Tau reflection nebula. Figure 23 shows spatial velocity cuts through the ^{12}CO data cube in which the horizontal axis is the radial velocity ranging from $V_{LSR} = -1.0 \text{ km s}^{-1}$ on the left to $V_{LSR} = +12.0 \text{ km s}^{-1}$ on the right. The vertical axis is the right ascension ranging from R.A. = 04:35:22.746 (68.8448) at the bottom of each panel to 04:36:22.790 (69.0950) at the top. Each panel is summed over a $75''$ range in declination. Panel 1 is the southernmost strip; Panel 9 is the northernmost strip. The right panel shows the locations of these two-dimensional spectra on a visual-wavelength image. Profiles of ^{12}CO and ^{13}CO are shown in Figure 24.

At radial velocities ranging from $V_{LSR} \sim 5$ to $\sim 6.25 \text{ km s}^{-1}$, the ^{12}CO emission is self-absorbed by a foreground layer of gas. The visibility of the reflection nebula at visual wavelengths implies that A_V through the foreground sheet cannot be more than a few magnitudes. G.J. Herczeg & L.A. Hillenbrand (2014) measured the extinction towards five of the young stars, finding a mean $A_V \sim 2.65$ mag, implying a column density of gas in front of the stars of a few times 10^{21} cm^{-2} . As shown in Figure 22, ^{12}CO emission at radial velocities which avoid the absorbing layer trace the visual appearance of the sharp, inner edges of the reflection nebula remarkably well. This indicates that the highest CO radial velocities coincide with the bright rims.

Figure 23 shows that Doppler-shifted emission from the shells protrudes on both the red- and blueshifted sides of the foreground gas. This emission can be seen at radial velocities between $V_{LSR} \sim 1.0$ to 5.3 km s^{-1} on the blueshifted side and between 6.7 and 8.0 km s^{-1}

on the redshifted side. The few km s^{-1} Doppler shifts are much smaller than what is generally associated with active outflows powered by forming stars. Our data does not show the outflow seen by G. Duvert et al. (2000) and associated with the star G2. Evidently this CO feature is too beam-diluted in our data to be seen by the $15''$ JCMT beam at our sensitivity.

The sharp, bright rim on the east, north, and west sides of the cavity is associated with ^{12}CO emission between $V_{LSR} = 2$ to 4 km s^{-1} . At $V_{LSR} = 4$ to 5 km s^{-1} , ^{12}CO emission traces emission extending $\sim 3'$ east of star G2 and $2'$ east of the cavity wall. The most blueshifted emission ($V_{LSR} \sim 1.8 \text{ km s}^{-1}$) in the HP Tau shells is located $2.7'$ east of KPNO 15 at 4:36:03.1, +22:52:48. A similar blueshifted region occurs on the west rim at 4:35:43.5, +22:53:47 about $2'$ northwest of KPNO15. These shells disappear behind the foreground gas at $V_{LSR} = 5$ to 6 km s^{-1} . The east, south, and west rims re-appear at $V_{LSR} = 6$ to 8 km s^{-1} on the redshifted side, with some knots filling-in the interior of the cavity (Figure 22e).

The ^{13}CO data cube probes the gas hidden by foreground ^{12}CO absorption. The upper panel of Figure 25 shows a three-color image of the ^{13}CO emission from $V_{LSR} = 4.7$ to 6.3 km s^{-1} . The brightest ^{13}CO emission originates from two spots (Peak 1 and 2) close to the central group of stars and associated with the brightest portion of the HP Tau reflection nebula. Peak 1 is $\sim 25''$ northwest of G2 and $\sim 10''$ north of HP Tau and has a peak brightness temperature of $\sim 2 \text{ K}$ in ^{13}CO . Peak 2 is $\sim 40''$ due west of G3 with a peak brightness temperature of also $\sim 2 \text{ K}$. At lower intensities between 0.3 to 0.7 K, diffuse ^{13}CO emission extends northwest from Peaks 1 & 2. The ^{13}CO emission peaks at $V_{LSR} = 5.9 \text{ km s}^{-1}$ (corresponding to $V_{hel} = 16.6 \text{ km s}^{-1}$).

The sharp inner rims of the reflection traced by ^{12}CO away from the absorbing layer are seen faintly in ^{13}CO with peak brightness temperatures up to $\sim 0.5 \text{ K}$. The eastern rim exhibits a narrow $\sim 1 \text{ km s}^{-1}$ -wide profile centered at $V_{LSR} \sim 4.3 \text{ km s}^{-1}$ with a fainter tail extending to about 6.5 km s^{-1} at some locations. The south, southwest, and east inner rims shift to $\sim 5.9 \text{ km s}^{-1}$ in ^{13}CO . Toward the south, these rims blend into the brighter South-East Rim near the bottom of Figure 1. The ^{13}CO emission from the South-East Rim reaches $\sim 1.7 \text{ K}$ and has median intensity of $\sim 1 \text{ K}$. In ^{12}CO , the South-East Rim is hidden by the foreground absorbing layer. Figure 25 shows that this clamshell feature is blueshifted with respect to Peak 1 by about 0.5 km s^{-1} . It has a radius of about $170''$ centered near Peaks 1 & 2 (Fig. 24).

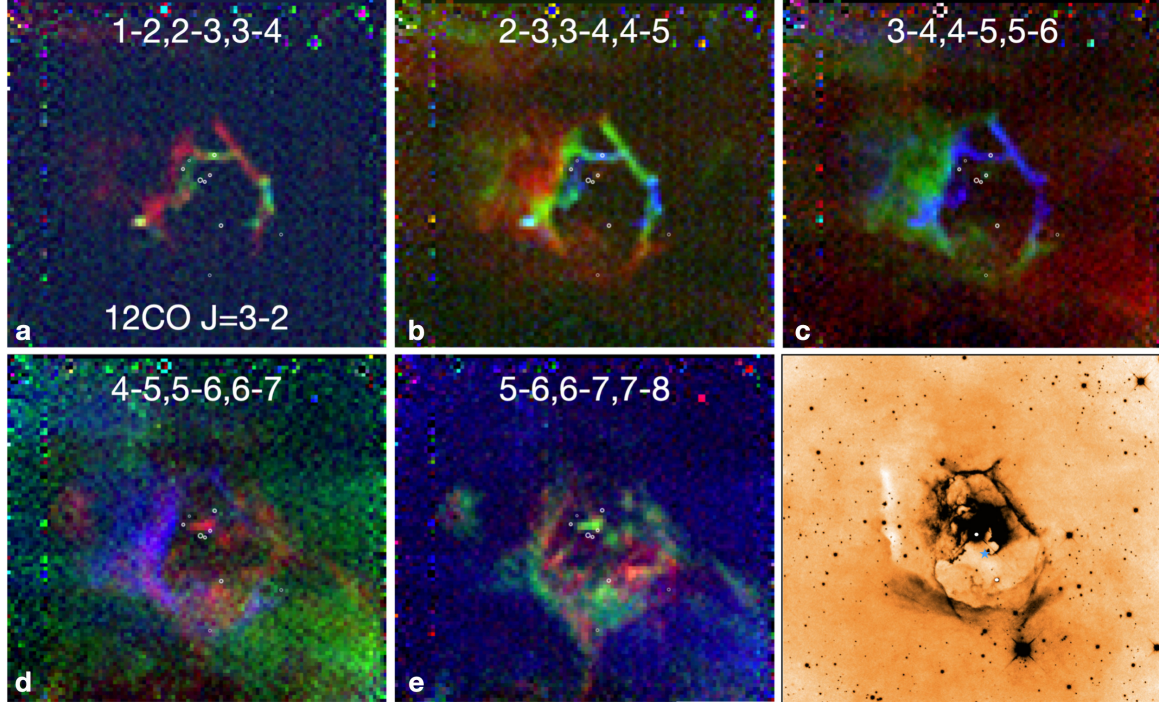


Figure 22. ^{12}CO $J=3-2$ in 5 channel maps displayed as three-color images in which three $\sim 1 \text{ km s}^{-1}$ -wide channels are shown in red, green, and blue, as indicated. Velocities are in local standard of rest. The peak of the CO emission is at $V_{\text{LSR}} = 5.93 \text{ km s}^{-1}$. The figure shows in finer detail the velocities of the cavity surrounding G2. The blue asterisk in the last panel shows where the triple system broke up, and the two white dots represent G2 and KPNO 15. The merger took place somewhere between the blue asterisk and the current position of G2.

The ^{13}CO morphology is similar to the sub-millimeter wave dust continuum traced by the $250 \mu\text{m}$ image (Figure 25).

9.3. Column Densities and Masses

We apply the X-factor method (Bolatto et al. 2013) as well as the RADEX code (van der Tak et al. 2007) to the estimation of ^{12}CO column densities. For the $J=3-2$ transition, Rigby et al. (2025) used column densities derived from Herschel Space Telescope sub-mm dust continuum observations and ^{12}CO and ^{13}CO observations of various regions in the Galaxy to derive $X_{^{12}\text{CO}3-2} = 4.0 \times 10^{20}$ and $X_{^{13}\text{CO}3-2} = 4.0 \times 10^{21} \text{ cm}^{-2} (\text{K km s}^{-1})^{-1}$. Thus, $N(\text{H}_2) = X \text{ I}_{\text{CO}} (\text{cm}^{-2})$ where I_{CO} is given by $\int T dV (\text{K km s}^{-1})$ and T is the brightness temperature in Kelvin in each species of CO and the integral is taken over the line profile in km s^{-1} . The mass in a region with area A is then given by $M = 2.7 m_H N(\text{H}_2) A$ where m_H is the mass of a hydrogen atom.

At radial velocities where most of the ^{13}CO emission is seen, ^{12}CO emission from the HP Tau shells are mostly hidden by the optically thick ^{12}CO foreground layer. We assume ^{13}CO is optically thin, and has an abundance relative to molecular hydrogen, $[^{13}\text{CO}] / [\text{H}_2] \approx 5 \times 10^{-6}$.

We use the X-factor and RADEX to estimate column densities and masses using ^{13}CO emission from Peaks 1 and 2 and the South-East Rim (the clamshell shaped arc in Figure 25). Peaks 1 and 2 are close to the stars illuminating the reflection nebula and heated by starlight. Acceptable RADEX solutions are obtained for gas temperatures ranging from 30 to 50 K and H_2 densities ranging from 10^3 to 10^4 cm^{-2} . The H_2 column densities range from 10^{21} to $3 \times 10^{21} \text{ cm}^{-2}$ and yield observed brightness temperatures of ~ 2 to 3 K for ^{13}CO . Mean radii of $12''$ for Peak 1 and $22''$ for Peak 2 imply masses of 0.006 to 0.018 M_\odot for Peak 1 and 0.02 to 0.06 M_\odot for Peak 2. The ^{13}CO X-factor method gives H_2 column densities of $4 \times 10^{21} \text{ cm}^{-2}$ and $6 \times 10^{21} \text{ cm}^{-2}$ for Peaks 1 and 2 which implies masses of 0.024 M_\odot and 0.12 M_\odot , respectively.

The shells seen at visual wavelengths protrude from behind the foreground veil at red- and blueshifted radial velocities in ^{12}CO . Some of these features can be faintly seen in ^{13}CO at $V_{\text{LSR}} \sim 3.6$ to 5 km s^{-1} on the blueshifted side of the absorbing layer, specifically from portions of the east, south, and west rims. The mean H_2 column densities in $18''$ by $106''$ boxes are 2×10^{20} , 8×10^{20} , and $6 \times 10^{20} \text{ cm}^{-2}$ corresponding to masses of 0.005, 0.02, and 0.015 M_\odot in the east, south, and west

rim. Thus, the total mass in these rims is at least $0.04 M_{\odot}$. This may be a severe lower bound limited by the faintness of the ^{13}CO emission.

The South-East Rim likely has lower gas temperature since it is located farther from the sources of illumination. For temperatures ranging from 10 to 25 K, and H_2 densities ranging from 10^3 to 10^4 cm^{-3} , H_2 column densities range from 3×10^{21} to 10^{22} cm^{-3} which yield brightness temperatures of 1 to 2 K. This implies a mass of 0.55 to $1.8 M_{\odot}$ for an effective area of 0.0084 square parsecs. The X-factor method gives a column density of $N(\text{H}_2) = 6 \times 10^{21} \text{ cm}^{-2}$ and mass $1.1 M_{\odot}$.

We use the X-factor method applied to ^{12}CO in a small $370''$ by $370''$ box centered on the cavity to estimate column densities and masses in two velocity ranges that exclude the foreground absorbing layer to estimate upper bounds. Between $V_{LSR} = 2.5$ and 5 km s^{-1} we find a mean column density $N(\text{H}_2) = 5 \times 10^{20} \text{ cm}^{-2}$ implying a mass of $0.9 M_{\odot}$. Between 6.5 and 8 km s^{-1} $N(\text{H}_2) = 4 \times 10^{20} \text{ cm}^{-2}$ implying a mass of $0.7 M_{\odot}$. These estimates include extended emission away from the sharp rims, and faint emission in the wings of the foreground layer $V_{LSR} 4$ to 5 km s^{-1} gas, and thus are severe upper bounds on the shell masses. Integrating over the entire line profile and using the X-factor method to a slightly smaller $690''$ by $690''$ (0.54 by 0.54 pc) region than mapped in both ^{13}CO and ^{12}CO , gives a mass of $5.8 M_{\odot}$ derived for ^{13}CO or $7.7 M_{\odot}$ derived from ^{12}CO . Most of this mass belongs to the foreground layer.

In summary, the mass in the inner shells, including Peaks 1 and 2, is between 0.1 and $0.3 M_{\odot}$. The mass of the south-east rim is 1 to $2 M_{\odot}$. The remaining mass belongs to the foreground layer and gas beyond the sharp rims.

9.4. Shell Morphology

The Magakian 77 reflection nebula associated with the HP Tau group consists of sharp, bright rims surrounding evacuated cavities. There are at least three partial shells: The bright inner half shell located within $\sim 30''$ of HP Tau, G2, and G3, the sharp-edged $\sim 130''$ by $300''$ diameter outer rim seen in Figure 1 and best seen in the blueshifted CO images, and finally the $^{13}\text{CO} \sim 160''$ radius South-East Rim clamshell feature seen in ^{13}CO and in the sub-mm dust emission.

As the stars accreted their masses a few Myr ago, they likely powered bipolar outflows which would have created cavities within the parent cloud at early times. Over 2 Myr the cavities left behind may have been filled-in and destroyed by turbulent motions within the parent cloud. Turbulent motions with an amplitude compa-

rable to the sound speed in cold molecular gas ($\sim 0.2 \text{ km s}^{-1}$), or larger, would have led cavity walls to expand and fill-in the cavities on a time-scale shorter than 0.5 Myr.

But the luminosity and T Tauri stellar winds emitted over ~ 2 Myr by young stars in the HP Tau compact group would have exerted sufficient radiation pressure to produce the cavities or to keep outflow-generated cavities open. While the merger flash is unlikely to have contributed much momentum, mass loss during a merger and its aftermath would likely have injected a strong pulse which could have created the sharp rims and cavity walls.

A spherical, expanding shell such as would be produced by an explosion is expected to have low radial velocities with respect to the host cloud at its projected edges located at the greatest projected distances from the expansion center. Radial velocity minima and maxima are expected towards the projected center of the shell. In the HP Tau region, the highest radial velocity deviations from the host cloud occur in or beyond the bright rims seen at visual wavelengths, not at the center of the cavity. This morphology is more consistent with a hole in a sheet of gas where the rims of the hole have been accelerated orthogonal to the plane of the sheet.

9.5. Did the Merger Create the Cavity & Shells?

The gravitational potential energy released by a merger of a star of mass m and radius r with a star of mass M and radius R is roughly given by

$$E_G \sim fGMm/(R+r)$$

where f is a parameter of order unity which depends on the final mass distribution within the merger remnant. For the merger of a $1 M_{\odot}$ and a $0.1 M_{\odot}$ star the energy release is of the order of a few times 10^{47} erg.

Note that E_G is orders of magnitude larger than the kinetic energy of motion in the walkaway stars. If G2 and KPNO15 have masses of 0.7 and $0.45 M_{\odot}$, and space motions of 5.7 and 9.3 km s^{-1} (see Table 2), their kinetic energies are 2.3×10^{44} ergs and 3.9×10^{44} ergs.

Mergers typically produce a luminous, transient flare lasting anywhere from weeks to years. The peak luminosity can range from 10^4 to over $10^7 L_{\odot}$. A class of red transients with luminosities between novae and supernovae (Luminous Red Novae) are thought to be powered by merging stars (Kasliwal et al. 2017; Karambelkar et al. 2023, 2025). Recent examples include V838 Mon (Limanets et al. 2023; T. Kamiński et al. 2021), V1309 Sco (R. Tyłenda & T. Kamiński 2016; T. Kamiński et al. 2015) (see Appendix F), and NGC 4490-OT2011 (Smith et al. 2016). The OMC1 cloud core behind the Orion

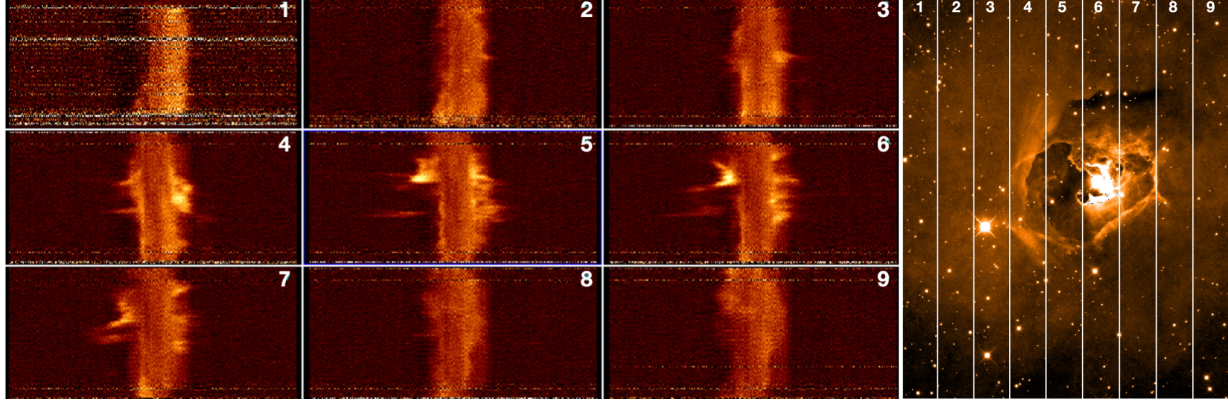


Figure 23. *left:* Spatial-velocity cuts through the ^{12}CO data cube, in which the horizontal axis is the radial velocity ranging from $V_{\text{LSR}} = -1.0 \text{ km s}^{-1}$ on the left to $V_{\text{LSR}} = +12.0 \text{ km s}^{-1}$ on the right. The vertical axis is the right ascension ranging from $\text{R.A.} = 04:35:22.746$ (68.8448) at the bottom of each panel to $04:36:22.790$ (69.0950) at the top. Each panel is summed over a $75''$ range in declination. Panel 1 is the southernmost strip; Panel 9 is the northernmost strip. *right:* The locations of the spatial-velocity strips are here shown on a visual-wavelength image. North is to the right, and East is up. Image courtesy Adam Block.

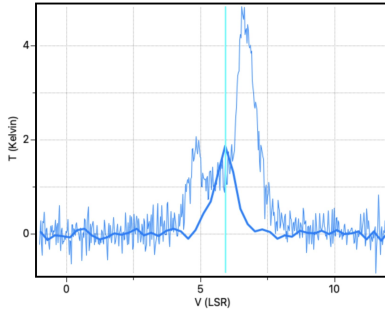


Figure 24. Profiles of ^{12}CO and ^{13}CO towards a circular area with radius 15.5 arcsec and centered at the position $4:35:53.1 +22:54:38$. The rest velocity of the cloud is $V_{\text{LSR}} = 5.93 \text{ km s}^{-1}$.

Nebula experienced a massive explosion, likely powered by a protostellar merger \sim 550 years ago (J. Bally et al. 2020).

Low-luminosity mergers with $M_V = -3$ or $M_I = -4$ are relatively common with a Galactic rate of order 0.5 to 0.3 yr^{-1} . Luminous mergers $M_V = -7$ or $M_I = -10$ have a rate of 0.03 yr^{-1} ; the peak luminosity scales as M^{2-3} . For massive stars, the peak luminosity is typically 10^2 to 10^4 times the main sequence luminosity of a star having the mass of the merger remnant (C.S. Kochanek et al. 2014).

The momentum in the flash is $P_{\text{rad}} = E_G/c$. For $M=1 \text{ M}_\odot$, $m=0.1 \text{ M}_\odot$, and $f=1$ it would be $P_{\text{rad}} \approx 9 \times 10^{36} \text{ erg cm s}^{-1}$ or $0.044 \text{ M}_\odot \text{ km s}^{-1}$. The maximum speed to which a shell with mass M_{shell} can be accelerated is $V_{\text{shell}} = P_{\text{rad}}/M_{\text{shell}}$, or

$$V_{\text{shell}} = f\eta GMm/cRM_{\text{shell}}$$

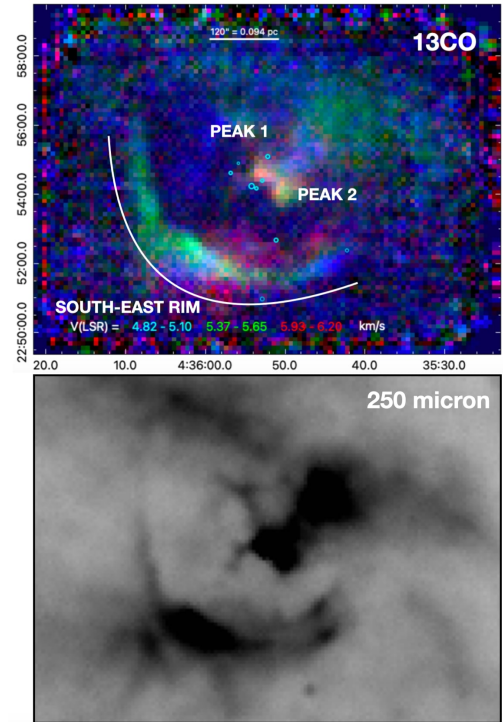


Figure 25. A ^{13}CO map of the region around the HP Tau group (upper panel). Emission from ^{13}CO is detected only between $4.96 < v_{\text{lsr}} < 6.50 \text{ km s}^{-1}$, and the figure is integrated over this velocity range. The lower panel is a Herschel $250 \mu\text{m}$ image. Both figures show the same area as the optical Figure 20.

where η is the fraction of the merger energy that goes into radiation during the transient. The total mass in the shells is estimated above to be ~ 0.1 to 1 M_\odot .

For $m=0.1 M_{\odot}$, $M=1 M_{\odot}$, $R = 10^{11}$ cm, $f=1$, $\eta=1$, and $V_{\text{shell}}=0.1 M_{\odot}$, the maximum speed would be only 0.44 km s^{-1} . But almost certainly, $\eta \ll 1$ since most of the energy of the merger is likely to be advected into the merger remnant rather than radiated away in a prompt flash. However, as the merger remnant settles toward the main sequence, the merger energy will emerge as radiation on a Kelvin-Helmholtz time-scale. Thus, unless the merger which produced G2 involved a pair stars more massive than $1 M_{\odot}$ each, the merger flash is unlikely to be responsible for forming the HP Tau cavities.

The total radiation emitted by the dozen stars in the HP Tau group over 2 Myr, however could have created the shells. The total mass in stars is at least several solar masses. The total radiation emitted by the gravitational contraction and formation of these stars is of order $E_g \sim GM^2/R > 3 \times 10^{48}$ erg where M is the total mass of the stars in the HP Tau group. We assume a severe lower-bound on the total mass of $M=1 M_{\odot}$ and use R from above as an effective radius. If radiated over 2 Myr, this energy could result in a mean luminosity of $\sim 10 L_{\odot}$. The maximum speed to which a shell with mass M_{shell} can be accelerated is $V_{\text{shell}} = E_g/cM_{\text{shell}}$. For $M_{\text{shell}}=0.1 M_{\odot}$, $V_{\text{shell}} \sim 4 \text{ km s}^{-1}$.

Young stars produce stellar winds. The mean mass-loss rate from young T-Tauri star winds is $\dot{M} \sim 10^{-9}$ to $10^{-8} M_{\odot} \text{ yr}^{-1}$ with a terminal wind velocity $V_w \sim 100$ to 200 km s^{-1} , the momentum delivered to the surrounding ISM over 1 Myr would be 0.1 to $2 M_{\odot} \text{ km s}^{-1}$. Thus, over 2 Myr, ten stars would deliver 2 to $40 M_{\odot} \text{ km s}^{-1}$.

Post-merger spectra show that merger remnants typically eject 1 to 10% of their mass with a speed of a few hundred km s^{-1} (T.R. Geballe et al. 2025; C.S. Kochanek et al. 2014). Since most observations are taken only a few years to decades after the merger, the ejecta may still be decelerating as they climb out of the remnant's gravitational potential well. The fraction that escapes may contribute momentum to the formation and acceleration of cavity walls.

If the G2 merger ejected a wind with a total mass $M_w \sim 0.01 M_{\odot}$ with a velocity at infinity of $V_w = 100 \text{ km s}^{-1}$, the momentum delivered by such a wind to the surrounding ISM is $P_w \sim 2 \times 10^{38} M_w \text{ erg cm s}^{-1}$ or $1 M_{\odot} \text{ km s}^{-1}$. For these parameters, and 1% of the merger remnant's $1 M_{\odot}$ mass ejected, the wind momentum would be much larger than the momentum in the merger's transient radiation. Thus, if mass loss from the G2 merger was similar to what is observed in other luminous red novae, the wind momentum would dominate over radiation.

The combined effects of protostellar bipolar outflows, radiation pressure, and T Tauri winds may have created and maintained the HP Tau cavities. Radiation pressure and winds from the G2 merger several thousand years ago could have created the sharp, arc-second scale rims surrounding the HP Tau cavities, and led to their acceleration to a speed of a few km s^{-1} .

10. SUMMARY AND CONCLUSIONS

1. We have carried out a detailed study of the bright T Tauri star HP Tau/G2, which is part of a little compact aggregate of 12 young stars and brown dwarfs associated with HP Tau. HP Tau/G2 is at the center of a peculiar shell-like reflection nebula.

2. Gaia proper motions show that HP Tau/G2 and KPNO 15, when referenced to the rest frame of the cloud, move straight away from each other with a tangential velocity difference of $\sim 14 \text{ km s}^{-1}$. These two walkaway stars were in a common point $\sim 5600 \text{ yr}$ ago. The ratio of proper motions for the two walkaway stars yields their mass ratio. Assuming a mass of $0.45 M_{\odot}$ for the M3 star KPNO 15 this suggests that HP Tau/G2 has a mass of $\sim 0.7 M_{\odot}$. This contrasts with the mass of $\sim 1.9 M_{\odot}$ derived from evolutionary tracks. Similarly the age of G2 of 3.6-5.0 Myr derived from evolutionary tracks is in conflict with the age of $2.0 \pm 0.3 \text{ yr}$ determined for the surrounding group of stars.

3. HP Tau/G2 is an unusual star. In addition to being a walkaway star, it is a weak-line T Tauri star with spectral type G2 with low-amplitude variability indicating the presence of spots. It also has an exceptionally large difference of 1400 K between temperatures derived in the optical and in the near-infrared. It is a fast rotator with a $v\sin i$ around 130 km s^{-1} and a period of 1.2 days, yielding a $rsini$ of $3.1 R_{\odot}$. For an estimated inclination of roughly 60° it follows that HP Tau/G2 has a large radius of $3.6 R_{\odot}$ and an oblate shape leading to significant gravity darkening. HP Tau/G2 is also a non-thermal radio source, indicating diffusive shock acceleration to mildly relativistic velocities, and it is an X-ray source. Finally, Gaia DR3 suggests that HP Tau/G2 may have a faint unresolved companion. While all these characteristics in isolation are not particularly remarkable, in combination they indicate a peculiar object.

4. In order to understand the nature of HP Tau/G2 we have been seeking guidance among late-type contact binaries and related stars. While W UMa stars have no resemblance to HP Tau/G2, we have found an almost perfect match with the evolved star FK Com. The FK Com stars form a small group of stars interpreted as mergers of contact binaries, and thus descendants of

W UMa stars. The similarity of HP Tau/G2 to the FK Com stars, its location at the center of a cavity, the discrepant mass from evolutionary tracks vs momentum conservation of the HP Tau/G2 and KPNO 15 walkaway pair, together with its unusual properties have led us to propose that HP Tau/G2 is a freshly spun-up merger remnant from the coalescence of two low-mass M-dwarfs or, more likely, an M-dwarf and a brown dwarf.

5. Coalescence of two stars in a binary can occur when the Darwin instability has been triggered. Tides will try to spin up the primary star at the expense of orbital angular momentum, but the spin of the orbit changes faster than the spin of the primary, so synchronization is never achieved. As a consequence the orbit shrinks and the primary spins up. At some point the stars may reach contact and the components will merge on an orbital time scale. Binaries with a very small mass ratio are much more likely to become Darwin unstable and merge.

6. Such a merger could be the result of the dynamical evolution in a higher-order multiple system of low-mass stars. It is impossible thousands of years later to say with any certainty how this chaotic process unfolded. During the protostellar phase random motions within an initially non-hierarchical configuration would after typically 100 crossing times lead to ejections into both bound orbits and escapes, mostly of low-mass objects. As a result of these ejections some of the remaining binaries became highly eccentric. In the presence of a dissipative environment the eccentric binaries could further tighten, especially during periastron passages, and begin to spiral in. The remaining stars would settle into a loosely bound and only marginally stable hierarchical architecture. Simulations show that such a system can survive for several million years and eject members, sometimes into escapes and sometimes again and again into very distant but bound orbits. In the case of HP Tau/G2 we speculate that after ~ 2 million yr the hierarchical but fragile multiple system was perturbed, internally or externally, leading to the near-simultaneous escape of KPNO 15 and HP Tau/G1 about ~ 5600 and ~ 4900 yr ago, respectively. As a result both the remaining HP Tau/G2 and HP Tau/G3 binaries were tightened, and in the case of HP Tau/G2 two of the three already tight components merged maybe ~ 2000 yr ago, while HP Tau/G3 ended up as a spectroscopic binary.

7. It is important to emphasize that, although the merger took place only a few thousand years ago, the dynamical evolution leading to this event was initiated already in the Class 0 or Class I protostellar phase, at a time when the multiple system was embedded and

possessed much circumstellar and circumbinary material that was continuously being replenished.

8. The actual merger could in principle have taken place at any time within the past ~ 5600 yr. We surmise that it occurred roughly 2000 yr ago, when HP Tau/G2 would have been near the center of the inner sharply outlined cavity. This is consistent with HP Tau/G2 cooling on a Kelvin-Helmholtz time scale, which is estimated at several thousand years, during which the star presumably could have observable peculiarities that would account for the current characteristics of the star. For an (uncertain) inclination of 60° HP Tau/G2 would be rotating at 77% of its breakup velocity and as a result would be very oblate, with a flattening R_p/R_{eq} of about 1.3, almost as much as the extreme case of the B3V star Achernar.

9. We have searched for additional stars with similar unusual properties as HP Tau/G2 and have found that another young star in Taurus, the luminous G5 weak-line T Tauri star HD 283572, is a near-twin. This may suggest that HP Tau/G2 is not a pathological case, but exemplifies an event that is not uncommon.

10. We speculate that G2 during its outburst might have appeared as an FU Ori event. The star FU Orionis is a luminous, bloated, fast rotating G2 star with a major polar spot. It has a massive disturbed disk which accounts for its large infrared excess and high luminosity. G2 is older, much less luminous, and presumably what might have been left of its disk was mostly obliterated in the merger explosion. While the outburst phase is long over, it is now in the process of re-organizing its interior to its new larger mass. We suggest that mergers form one more of several mechanisms that may cause FU Ori-like outbursts.

11. The reflection nebula surrounding the HP Tau group shows three partial shells with sharp inner edges. ^{12}CO and ^{13}CO observations reveal that the gas is currently slowly expanding, possibly but not necessarily triggered by an explosion.

12. We cannot *prove*, several thousand years later, that HP Tau/G2 suffered a merger, but we believe we have presented evidence that makes this *a highly probable event*. We recognize that there are a number of unresolved issues and uncertainties which may be addressed by Gaia DR4 and by further observations.

ACKNOWLEDGEMENTS

We thank the referee for helpful comments. We are also thankful to Christoph Baranec, Fernando Comerón, Claus Fabricius, Lynne Hillenbrand, Ward

Howard, Daniel Huber, Tomasz Kamiński, Nathan Leigh, Kevin Luhman, André Maeder, Slavek Rucinski, Fabian Schneider, Alison Sills, Andrei Tokovinin, Romuald Tylenda, Watson Varricatt, and Miguel Vioque for help and insightful comments.

We thank Adam Block for the optical image in Figures 3, 20, 22, and 23, Vardan Elbakyan for use of Figure 19, Alexandr Zaytsev and Mark Hanson for the image in Figure 1, and Cédric Mauro and Christophe Marsaud from Team Astrofleet for Figure 17.

This work has made use of data from the European Space Agency (ESA) mission *Gaia* (<https://www.cosmos.esa.int/gaia>), processed by the *Gaia* Data Processing and Analysis Consortium (DPAC, <https://www.cosmos.esa.int/web/gaia/dpac/consortium>). Funding for the DPAC has been provided by national institutions, in particular the institutions participating in the *Gaia* Multilateral Agreement. The work presented here is based in part on observations obtained with the Apache Point Observatory 3.5-meter telescope, which is owned and operated by the Astrophysical Research Consortium. We thank the Apache Point Observatory Observing Specialists for their assistance during the observations. The NASA Infrared Telescope Facility is operated by the University of Hawaii under contract 80HQTR24DA010 with the National Aeronautics and Space Administration. MSC is a Visiting Astronomer at the Infrared Telescope Facility, which is operated by the University of Hawaii under contract 80HQTR19D0030 with the National Aeronautics and Space Administration. Based in part by observations at the Southern Astrophysical Research (SOAR) telescope, which is a joint project of the Ministerio da Ciencia, Tecnologia e Inovacoes do Brasil (MCTI/LNA), the US National Foundation's NOIRLab, the University of North Carolina at Chapel Hill (UNC), and Michigan State University (MSU). The James Clerk Maxwell Telescope is operated by the East Asian Observatory on behalf of The National Astronomical Observatory of Japan; Academia Sinica Institute of Astronomy and Astrophysics; the Ko-

rea Astronomy and Space Science Institute; the Operation, Maintenance and Upgrading Fund for Astronomical Telescopes and Facility Instruments, budgeted from the Ministry of Finance (MOF) of China and administrated by the Chinese Academy of Sciences (CAS), as well as the National Key R&D Program of China (No. 2017YFA0402700). Additional funding support is provided by the Science and Technology Facilities Council of the United Kingdom and participating universities in the United Kingdom and Canada. Program ID M18BH13A. This paper includes data collected by the Kepler mission and obtained from the MAST data archive at the Space Telescope Science Institute (STScI). Funding for the Kepler mission is provided by the NASA Science Mission Directorate. STScI is operated by the Association of Universities for Research in Astronomy, Inc., under NASA contract NAS 5-26555. This paper includes data collected by the TESS mission, which are publicly available from the Mikulski Archive (MAST). This paper has used archival data from the Herschel mission. Herschel is an ESA space observatory with science instruments provided by European-led Principal Investigator consortia and with important participation from NASA. This research has made use of the SIMBAD database, operated at CDS, Strasbourg, France, and of NASA's Astrophysics Data System Bibliographic Services. J.B. acknowledges support by National Science Foundation through grant No. AST-1910393.

Facilities: JCMT(HARP), SOAR (GHTS, Triple-Spec), APO(NICFPS), IRTF (SpeX, iSHELL), Keck(HIRES), ASAS-SN, TESS, HST(WFCM2)

Software: CASA (CASA Team et al. 2022); IRAF (D. Tody 1986, 1993); PyRAF (Science Software Branch at STScI 2012); Anaconda Python (Anaconda Software Distribution 2020); DS9 (W. Joye & E. Mandel 2003) Lightkurve (Lightkurve Collaboration et al. 2018)

REFERENCES

Afsar, M. & Bond, H.E. 2007, AJ, 133, 387
 Andrews, S.M. 2020, ARAA, 58:483
 Anglada, G. 1996, ASPC, 93, 3
Anaconda Documentation 2020. Anaconda Inc. Retrieved from <https://docs.anaconda.com/>
 Anosova, J.P. 1986, Astrophys. Spa.Sci., 124, 217
 Aspin, C., Reipurth, B. 2000, MNRAS, 311, 522
 Arce, H., Borkin, M.A., Goodman, A.A. et al. 2011, ApJ, 742, A105
 Ayres, T.R., Kashyap, V., Huenemoerder, D. et al. 2016, ApJS, 223:5
 Badalian, G.S. 1961, Astron. Tsirk., 224, 22
 Bally, J., Ginsburg, A., Forbrich, J., et al. 2020, ApJ, 889, 2, 178. doi:10.3847/1538-4357/ab65f2
 Balona, L.A. 2018, Front. Astron. Space Sci. 5:43 doi: 10.3389/fspas.2018.00043
 Baraffe, I., Homeier, D., Allard, F., Chabrier, G. 2015, A&A, 577, A42

Bate, M.R., Bonnell, I.A., Bromm, V. 2002, MNRAS, 336, 705

Benz, W. & Hills, J.G. 1987, ApJ, 323, 614

Bessell, M.S. & Brett, J.M. 1988, PASP, 100, 1134

Bieging, J.H., Cohen, M., Schwartz, P.R. 1984, ApJ, 282, 699

Blaauw, A. 1961, Bull. Astron. Inst. Netherlands, 15, 265

Bolatto, A. D., Wolfire, M., & Leroy, A. K. 2013, ARA&A, 51, 1, 207. doi:10.1146/annurev-astro-082812-140944

Bonnell, I. & Bastien, P. 1992, ApJ, 401, L31

Bopp, B.W. & Rucinski, S.M. 1981, in IAU Symp. No. 93, p.177B

Bopp, B.W. & Stencel, R.E. 1981, ApJ, 247, L131

Borchert, E.M.A., Price, D. pinte, C., Cuello, N. 2022, MNRAS, 517, 4436

Bouvier, J., Covino, E., Kovo, O. et al. 1995, A&A, 299, 89

Bowman, D.M. & Bugnet, L. 2026, Encyclopedia of Astrophysics, Vol. 2, Elsevier, pp. 133-153

Briceño, C., Luhman, K.L., Hartmann, L. et al. 2002, ApJ, 580:317

Briceño, C., Calvet, N., Hernandez, J., et al. 2019, AJ, 157, 85

Briceño, C., Luhman, K.L., Hartmann, L., Stauffer, J.R., Kirkpatrick, J.D. 2002, ApJ, 580, 317

CASA Team, Bean, B., Bhatnagar, S. et al. 2022, in PASP, Vol. 134, issue 1041, id.114501

Cifuentes, C, Caballero, J.A., González-Payo, J. et al. 2025, A&A, 693, A228

Claret, A. 2012, A&A, 538, A3

Clemens, J. C., Crain, J. A., & Anderson, R. 2004, in Proc. SPIE, Vol. 5492, *Ground-based Instrumentation for Astronomy*, ed. A. F. M. Moorwood & M. Iye, 331-340

Cody, A.M., Hillenbrand, L., Rebull, L. 2022, AJ, 163, A212

Cohen, M. & Bieging, J.H. 1986, AJ, 92, 1396

Cohen, M. & Kuhi, L.V. 1979, ApJ Suppl. 41, 743

Connelley, M.S., Reipurth, B., Tokunaga, A.T. 2007, AJ, 133, 1528

Connelley, M.S., Reipurth, B., Tokunaga, A.T. 2008a, AJ, 135, 2496

Connelley, M.S., Reipurth, B., Tokunaga, A.T. 2008b, AJ, 135, 2526

Contreras Peña, C., Lee, J.-E., Herczeg, G. et al. 2025, arXiv:2509.24876

Cushing, M. C., Vacca, W. D., & Rayner, J. T. 2004, PASP, 116, 362. doi:10.1086/382907

Dahm, S.E. & Hillenbrand, L.A. 2017, AJ, 154, 177

Darwin, G.H. 1879, Proc. Roy. Soc. London, 29, 168

Davies, C.L., Gregory, S.G., Greaves, J.S. 2014, MNRAS 444, 1157

de Mink, S.E., Sana, H., Langer, N. et al. 2014, ApJ, 782:7

Domiciano de Souza, A., Kervella, P., Moser Faes, D. et al. (2014), A&A, 569, A10

Donati, J.-F., Semel, M., Carter, B.D. et al. 1997, MNRAS, 291, 658

Dopita, M.A. 1978, ApJS, 37, 117

Drake, J.J., Chung, S.M., Kashyap, V., Korhonen, H. et al. 2008, ApJ, 679:1522

Duvert, G., Guilloteau, S., Ménard, F. et al. 2000, A&A, 355, 165

Eggleton, P.P. & Kiseleva-Eggleton, L. 2001, ApJ, 562, 1012

Elbakyan, V.G., Vorobyov, E.I., Rab, C. et al. 2019, MNRAS, 484, 146

Farias, J.P., Tan, J.C., Eyer, L. 2020, ApJ, 900:14

Espinosa Lara, F. & Rieutord, M. 2011, A&A, 533, A43

Favata, F., Micela, G., Sciortino, S. 1998, A&A, 337, 413

Feigelson, E. & Kriss, J. 1981, ApJ, 248, L35

Fernandez, M. & Miranda, L.F. 1998, A&A, 332, 629

Ferrario, L., Pringle, J.E., Tout, C.A., Wickramasinghe, D.T. 2009, MNRAS, 400, L71

Fitton, S., Tofflemire, B.M., Kraus, A.L. RNAAS, 6, 18

Flores, C., Connelley, M.S., Reipurth, B., Boogert, A. 2019, ApJ, 882:75

Flores, C., Reipurth, B., Connelley, M.S. 2020, ApJ, 898, 109

Flores, C., Connelley, M.S., Reipurth, B. 2022, ApJ, 925:21

Furlan, E., Fischer, W.J., Ali, B. et al. 2016, ApJS, 224, 5

Gaia collaboration, Prusti, T., de Bruijne, J.H.J. et al. 2016, A&A, 595, A1

Gaia collaboration, Brown, A.G.A., Vallenari, A. et al. 2021, A&A, 649, A1

Galli, P.A.B., Loinard, L., Ortiz-Léon, G.N. et al. 2018, ApJ, 859:33

Garufi, A., Ginski, C., van Holstein, R.G., Benisty, M., Manara, C.F. et al. 2024, A&A, 685, A53

Garufi, A., Carrasco-Gonzalez, C., Macias, E. et al. 2025, A&A, 694, A290

Geballe, T. R., Kaminski, B. M., Banerjee, D. P. K., et al. 2025, MNRAS, 541, 4, 3331. doi:10.1093/mnras/staf1193

Graham, J.A. & Frogel, J.A. 1985, ApJ, 289, 331

Grankin, K.N., Bouvier, J., Herbst, W., Melnikov, S.Yu. 2008, A&A, 479, 827

Güdel, M., Briggs, K.R., Arzner, K. et al. 2007, A&A, 468, 353

Guieu, S., Dougados, C., Monin, J.-L., Magnier, E., Martin, E.L. 2006, A&A, 446, 485

Guinan, E.F. & Robinson, C.R. 1986, AJ, 91, 935

Guo, Y.-X., Luo, A.-L., Zhang, S., Du, B., Wang, Y.-F. et al. 2019, MNRAS, 485, 2167

Haro, G. 1953, ApJ, 117, 73

Hartigan, P., Strom, K.M., Strom, S.E. 1994, ApJ, 427, 961

Hartmann, L., Hewett, R., Stahler, S., and Mathieu, R.D. 1986, *ApJ*, 309, 275

Hartmann, L., Herczeg, G., Calvet, N. 2016, *ARAA*, 54, 135

Henneco, J., Schneider, F.R.N., Laplace, E. 2024, *A&A*, 682, A169

Henriksen, R.N., Ptuskin, V.S., Mirabel, I.F. 1991, *A&A*, 248, 221

Herbig, G.H. 1977, *ApJ*, 217, 693

Herbig, G.H. 1989, in *Low Mass Star Formation and Pre-main Sequence Objects*, ESO Conf. Proc. 33, ed. Bo Reipurth, p.233

Herbig, G.H. & Rao, N.K. 1972, *ApJ*, 174, 401

Herbig, G.H., Petrov, P.P., Duemmler, R. 2003, *ApJ*, 595, 384

Herbst, W. 1986, *PASP*, 98, 1088

Herczeg, G.J. & Hillenbrand, L.A. 2014, *Ap*, 786, A97

Hillenbrand, L.A., De, K., Hankins, M. et al. 2021, *AJ*, 161:220

Hillenbrand, L.A., Isaacson, H., Rodriguez, A.C. et al. 2022, *AJ*, 163:115

Hillenbrand, L.A., Carvalho, A., van Roestel, J., De, K. 2023, *ApJ*, 958:L27

Hills, J.G. & Day, C.A. 1976, *Astrophys. Lett.*, 17, 87

Hubble, E.P. 1916, *ApJ*, 44, 190

Hut, P. 1981, *A&A*, 99, 126

Huenemoerder, D.P., Ramsey, L.W., Buzasi, D.L., Nations, H.L. 1993, *ApJ*, 404, 316

Ibragimov, M.A. 1993, *ARep*, 37, 1761

MNRAS, 474, 1176

Jetsu, L., Pelt, J., Tuominen, I. 1993, *A&A*, 278, 449

Johns-Krull C.M. 1996, *A&A*, 306, 803

Joncour, I., Bertout, C., Bouvier, J. 1994, *A&A*, 291, L19

Joncour, I., Duchêne, G., Moraux, E. et al. 2018, *A&A*, 620, A27

Jönsson, H., Holtzman, J.A., Allende Prieto, C. et al. 2020, *AJ*, 160:120

Jones, B.F. & Herbig, G.H. 1979, *AJ*, 84, 1872

Joye, W.A. & Mandel 2003, in *Astronomical Data Analysis Software and Systems XII*, ASP Conference Series, Vol. 295, H. E. Payne, R. I. Jedrzejewski, and R. N. Hook, eds., p.489

Kamiński, T., Mason, E., Tylenda, R., et al. 2015, *A&A*, 580, A34. doi:10.1051/0004-6361/201526212

Kamiński, T., Menten, K. M., Tylenda, R., et al. 2020, *A&A*, 644, A59. doi:10.1051/0004-6361/202038648

Kamiński, T., Tylenda, R., Kiljan, A. et al. 2021, *A&A*, 655, A32. doi:10.1051/0004-6361/202141526

Karambelkar, V. R., Kasliwal, M. M., Blagorodnova, N., et al. 2023, *ApJ*, 948, 2, 137. doi:10.3847/1538-4357/acc2b9

Karambelkar, V., Kasliwal, M., Lau, R. M., et al. 2025, , arXiv:2508.03932. doi:10.48550/arXiv.2508.03932

Kasliwal, M. M., Bally, J., Masci, F., et al. 2017, *ApJ*, 839, 2, 88. doi:10.3847/1538-4357/aa6978

Kenyon, S.J. & Hartmann, L. 1995, *ApJS*, 101, 117

Kerr, R.M.P., Rizzuto, A.C., Kraus, A.L., Offner, S.S.R. 2021, *ApJ*, 917, 23

Kipper, T., Klochkova, V.G., Annuk, K. et al. 2004, *A&A*, 416, 1107

Kiseleva, L.G., Eggleton, P.P., Mikkola, S. 1998, *MNRAS*, 300, 292

Kjurkchieva, D.P. & Marchev, D.V. 2005, *A&A*, 434, 221

Knox-Shaw, H. 1916, *MNRAS*, 76, 646

Kochanek, C.S., Adams, S.M., Belczynski, K. 2014, *MNRAS*, 443, 1319

Kochanek, C.S., Shappee, B.J., Stanek, K.Z. et al. 2017, *PASP*, 129, 104502 doi:10.1093/mnras/stu1226

Kopal, Z. 1959, *Close Binary Stars*, Chapman & Hall, London

Korhonen, H., Berdyugina, S.V., Hackman, T. et al. 1999, *A&A*, 346, 101

Korhonen, H., Berdyugina, S.V., Hackman, T. et al. 2000, *A&A*, 360, 1067

Korhonen, H., Berdyugina, S.V., Hackman, T. et al. 2007, *A&A*, 476, 881

Korhonen, H., S. Hubrig, Berdyugina, S.V. et al. 2009, *MNRAS*, 395, 282

Kraus, A.L., Ireland, M.J., Martinache, F. et al. 2011, *ApJ*, 731, A8

Krolikowski, D.M., Krays, A.L., Rizzuto, A.C. 2021, *AJ*, 162:110

Larson, R.B. 1980, *MNRAS*, 190, 321

Lee, A.T., Offner, S.S.R., Kratter, K.M. et al. 2019, *ApJ*, 887, 232

Leigh, N.W.C., Geller, A.M., Shara, M.M. 2017, *MNRAS*, 471, 1830

Leigh, N.W.C., Geller, A.M., Shara, M.M. 2018, *MNRAS*, 480, 3062

Leiner, E., Mathieu, R.D., Vanderburg, A. et al. 2019, *ApJ*, 881:47

Leinert, Ch., Zinnecker, H., Weitzel, N. et al. 1993, *A&A*, 278, 129

Li, H., Li, D., Xu, D., Goldsmith, P.F. et al. 2015, *ApJS*, 219:20

Lightkurve Collaboration et al. 2018, *Astrophysics Source Code Library*, <https://ui.adsabs.harvard.edu/abs/2018ascl.soft12013L/abstract>

Liimets, T., Kolka, I., Kraus, M., et al. 2023, *A&A*, 670, A13. doi:10.1051/0004-6361/202142959

Lin, C.-L. Ip, W.-H., Chang, T.-H., Song, Y., Luo, A.-L. 2023, AJ, 166:82

Lovell, J.B., Keating, G.K., Wilner, D.J. et al. 2024, ApJ, 962:L12

Lucy, L.B. 1967, Z.f.Ap. 65, 89

Luhman, K.L. 2018, AJ, 156, A271

Luhman, K.L. 2023, AJ, 165:37

Luhman, K.L. 2025, AJ, 170, 19

Luhman, K.L., Briceno, C., Stauffer, J.R., Hartmann, L., Barrado y Navascues, D., Caldwell, N. 2003, ApJ, 590:348

Luhman, K.L., Mamajek, E.E., Allen, P.R., Cruz, K.L. 2009, ApJ, 703, 399

Luhman, K.L., Allen, P.R., Espaillat, C. et al. 2010, ApJS, 186, 111

Luhman, K.L., Mamajek, E.E., Shukla, S.J., Loutrel, N.P. 2017, AJ, 153, 46

MacLeod, M., Ostriker, E.C., & Stone, J.M. 2018, ApJ, 868:136

Maeder, A. 2009, *Physics, Formation and Evolution of Rotating Stars* (Berlin:Springer)

Magakian, T. Yu. 2003, A&A, 399, 141
ApJ, 628, 439

Malo, L., Artigau, E., Doyon, R. et al. 2014, ApJ, 788, A81

Mathieu, R.D., Stassun, K., Basri, G. et al. 1997, AJ, 113, 1841

Mathieu, R.D. & Pols, O.R. 2025, ARAA, 63-467

Mason, E., Shore, S.N. 2022, A&A, 664, A12

Mason, E., Williams, R.E., Preston, G., Bensby, T. 2010, A&A, 516, A108

McBride, A. & Kounkel, M. 2019, ApJ, 884:6

Mohan, S., Vig, S., Mandal, S. 2022, MNRAS, 514, 3709

Moriarty-Schieven, G.H., Wannier, P.G., Tamura, M., Keene, J. 1992, ApJ, 400, 260

Mullan, D.J. & MacDonald, J. 2020, ApJ, 904:108

Munari, U., Henden, A., Kiyota, S. et al. 2002, A&A, 389, L51

Nandez, J.L.A., Ivanova, N., Lombardi, J.C. 2014, ApJ, 786:39

Naoz, S. & Fabrycky, D.C. 2014, ApJ, 793:137

Narayanan, G., Heyer, M.H., Brunt, C. et al. 2008, ApJS, 177:341

Narayanan, G., Snell, R., Bemis, A. 2012, MNRAS, 425, 2641

Nguyen, D.C., Brandeker, A., van Kerkwijk, M.H., Jayawardhana, R. 2012, ApJ, 745, A119

Offner, S.S.R., Moe, M., Kratter, K.M. et al. 2023, in *Protostars and Planets VII*, S. Inutsuka et al., eds.

Oliveira, J.M. & Foing, B.H. 1999, A&A, 343, 213

O'Neal, D., Feigelson, E.D., Mathieu, R.D., Myers, P.C. 1990, AJ, 100, 1610

Panov, K. & Dimitrov, D. 2007, A&A, 467, 229

Patterer, R.J., Ramsey, L., Welty, A.D., Huenemoerder, D.P. 1993, AJ, 105, 1519

Perets, H.B. *Evolution of Triple Stars*, in Encyclopedia of Astrophysics Vol.2, ed. I. Mandel (Editor-in-Chief), Elsevier, p.279-297

Perets, H.B. & Fabrycky, D.C. 2009, ApJ, 697, 1048

Petrov, P.P. & Herbig, G.H. 1992, ApJ, 392, 209

Petrov, P.P. & Herbig, G.H. 2008, AJ, 136, 676

Platais, I., Robberto, M., Bellini, A. et al. 2020, AJ, 159:272

Pouilly, K., Bouvier, J., Alecian, E., Alencar, S.H.P., Cody, A.M. et al. 2020, AA, 642, A99

Purser, S.J.D., Ainsworth, R.E., Ray, T.P. et al. 2018, MNRAS, 481, 5532

Raga, A.C., Canto, J., Binette, L., Calvet, N. et al. 1990, ApJ, 364, 601

Ramsey, L.W., Nations, H.L., Barden, S.C. 1981, ApJ, 251, L101

Rawiraswattana, K., Lomax, O., & Goodwin, S.P. 2012, MNRAS, 419, 2025

Ray, T.P., Muxlow, T.W.B., Brown, A. et al. 1997, Nature, 385, 415

Rayner, J., Tokunaga, A., Jaffe, D. et al. 2022, PASP, 134, 015002

Rebull, L.M., Makidon, R.B., Strom, S.E. et al. AJ, 123, 1528

Rebull, L.M., Wolff, S.C., Strom, S.E. 2004, AJ, 127, 1029

Rebull, L.M., Stauffer, J.R., Cody, A.M., Hillenbrand, L.A., Bouvier, J. et al. 2020, AJ, 159:273

Reipurth, B. 1985, A&A, 143, 435

Reipurth, B. 2000, AJ, 120, 3177

Reipurth, B. & Bally, J. 1986, Nature, 320, 336

Reipurth, B. & Aspin, C. 2004, ApJ, 608, L65

Reipurth, B., Mikkola, S., Connelley, M., Valtonen, M. 2010, ApJ, 725, L56

Reipurth, B. & Mikkola, S. 2012, Nature, 492, 221

Reipurth, B. & Mikkola, S. 2015, AJ, 149, A145

Reipurth, B., Herbig, G.H., Bally, J. et al. 2018, AJ, 156, A25

Renzo, M., Zapartas, E., de Mink, S.E. et al. 2019, A&A, 624, A66

Reynolds, S.P. 1986, ApJ, 304, 713

Richichi, A., Leinert, Ch., Jameson, R., Zinnecker, H. 1994, A&A, 287, 145

Rieke, G.H. & Lebofsky, M.J. 1985, ApJ, 288, 618

Rivera, J.L., Loinard, L., Dzib, S.A. et al. 2015, ApJ, 807, 119

Rizzuto, Aaron C.; Dupuy, Trent J.; Ireland, Michael J.; Kraus, Adam L. 2020, ApJ, 889, A175

Rigby, A. J., Thompson, M. A., Eden, D. J., et al. 2025, MNRAS, 538, 1, 198. doi:10.1093/mnras/staf278

Rodriguez, J.E., Ansdell, M., Oelkers, R.J., Cargile, P.A., Gaidos, E. et al. 2017, ApJ, 848:97

Rodriguez, L.F., Curiel, S., Moran, J.M. et al. 1989, ApJ, 346, L85

Rucinski, S.M. 1990, PASP, 102, 306

Rucinski, S.M. 1991, AJ, 101, 2199

Rucinski, S.M., Pribulla, T., van Kerkwijk, M.H. 2007, AJ, 134, 2353

Rudy, R.J. Lynch, D.K., Russell, R.W. et al. 2008a, IAUC 8976

Rudy, R.J. Lynch, D.K., Russell, R.W. et al. 2008b, IAUC 8997

Ryu, T., Sills, A., Pakmor, R. et al. 2025, ApJL, 980:L38

Savanov, I.S., Naroenkov, S.A., Nalivkin, M.A., Dmitrienko, E.S. 2023, Astron. Rep. 67, 1394

Scelsi, L., Maggio, A., Micela, G. et al. 2007, A&A, 468, 405

Scelsi, L., Sacco, G., Affer, L. et al. 2008, A&A, 490, 601

Schneider, F.R.N. 2025, arXiv:2509.18421

Schneider, F.R.N., Ohlmann, S.T., Podsiadlowski, Ph. et al. 2019, Nature, 574, 211

Schneider, F.R.N., Ohlmann, S.T., Podsiadlowski, Ph. et al. 2020, MNRAS, 495, 2796

Schoettler, C., Parker, R.J., Arnold, B. et al. 2019, MNRAS, 487, 4615

Science Software Branch at STScI 2012, Astrophysics Source Code Library, record ascl:1207.011

Seidl, F.G.P. & Cameron, A.G.W. 1972, Ap&SS, 15, 44

Serna, J., Hernandez, J., Kounkel, M. et al. 2021, ApJ, 923:177

Shappee, B., Prieto, J.L., Grupe, D. et al. 2014, ApJ, 788, 48

Shariat, C., Naoz, S., Hansen, B.M.S. et al 2023, ApJL, 955:14

Shariat, C., Naoz, S., El-Badry, K. et al. 2025, ApJ, 978:47

Simon, M., Howell, R.R., Longmore, A.J. et al. 1987, ApJ, 320, 344

Simon, M., Ghez, A.M., Leinert, Ch. et al. 1995, ApJ, 443, 625

Siwak, M., Rucinski, S.M., Matthews, J.M. et al. 2011, MNRAS, 415, 1119

Smith, N., Andrews, J. E., Van Dyk, S. D., et al. 2016, MNRAS, 458, 1, 950. doi:10.1093/mnras/stw219

Soker, N. & Tylenda, R. 2003, ApJ, 582, L105

Soker, N. & Tylenda, R. 2006, MNRAS, 373, 733

Stahler, S.W. 2010, MNRAS 402, 1758

Stassun, K.G., Mathieu, R.D., Mazeh, T. Vrba, F.J. 1999, AJ, 117:2941

Stassun, K.G., Mathieu, R.D., Vrba, F.J. et al. 2001, AJ, 121, 1003

Steinmetz, T., Kamiński, T., Schmidt, M., Kiljan, A. 2024, A&A, 682, A127

Stepień, K. 2011, A&A, 531, A18

Sterzik, M.F. & Durisen, R.H. 1995, A&A, 304, L9

Strassmeier, K.G. 2009, A&A Rev. 17:251

Strassmeier, K.G. & Rice, J.B. 1998, A&A, 339, 497

Strom, K.M. & Strom, S.E. 1993, ApJ, 412, L63

Strom, K.M. & Strom, S.E. 1994, ApJ, 424, 237

Strom, K.M. et al. 1986 ApJ Supp. 62, 39

Struve, O. & Straka, W.C. 1962, PASP, 74, 474

Szabó, Zs.M., Kospal, A., Abraham, P. et al. 2021, ApJ, 917, 80

Tetzlaff, N., Neuhäuser, R., Hohle, M.M. 2011, MNRAS, 410, 190

Tobin, J.J., Offner, S.S.R., Kratter, K.M. et al. (2022) ApJ, 925:39

Tody, D. 1986, in *Instrumentation in astronomy VI*; Proceedings of the Meeting, Tucson, AZ, Mar. 4-8, 1986. Part 2 (A87-36376 15-35). Bellingham, WA, Society of Photo-Optical Instrumentation Engineers, 1986, p. 733.

Tody, D. 1993, in *Astronomical Data Analysis Software and Systems II* (1993), A.S.P. Conference Series, Vol. 52, R. J. Hanisch, R. J. V. Brissenden, and Jeannette Barnes, eds., p. 173.

Tokovinin, A. 2021, Universe, 7, 352

Tokovinin, A. & Moe, M. 2020, MNRAS, 491, 5158

Tokovinin, A., Thomas, S., Sterzik, M., Udry, S. 2006, A&A, 450, 681

Toonen, S., Boekholt, T.C.N., Portegies Zwart, S. 2022, A&A, 661, A61

Torres, R.M., Loinard, L., Mioduszewski, A.J., Rodriguez, L.F. 2007, ApJ, 671:1813

Torres, R.M., Loinard, L., Mioduszewski, A.J., Rodriguez, L.F. 2009, ApJ, 698, 242

Tylenda, R. & Kamiński, T. 2016, A&A, 592, A134 doi:10.1051/0004-6361/201527700

Tylenda, R., Hajduk, M., Kamiński, T. et al. 2011, A&A, 528, A114

Vallii, R., Tiede, C., Vigna-Gómez, A. et al. 2024, A&A, 688, A128

Valtonen, M. & Mikkola, S. 1991, Ann. Rev. Astron. Astrophys., 29, 9

van der Marel, N. 2023, Eur. Phys. J. Plus, 138, 225

van der Tak, F. F. S., Black, J. H., Schöier, F. L., et al. 2007, A&A, 468, 2, 627. doi:10.1051/0004-6361:20066820

Vasilyev, V., Reinhold, T., Shapiro, A. et al. 2024, Science, 386, 1301

Vida, K., Korhonen, H., Ilyin, I.V. et al. 2015, *A&A*, 580, A64

von Zeipel, H. 1924, *MNRAS*, 84, 665

Vorobyov, E.I., Elbakyan, V.G., Hosokoawa, T. et al. 2017, *A&A*, 605, A77

Vorobyov, E.I., Elbakyan, V.G., Liu, H.B., Takami, M. 2021, *A&A*, 647, A44

Vrba, F.J., Rydgren, A.E., Chugainov, P.F., Shakovskaya, N.I., Weaver, W.B. 1989, *AJ*, 97, 483

Vynatheya, P., Ryu, T., Wang, C. et al. 2025, arXiv:2510.13736

Walter, F.M. & Kuhf, L.V. 1981, *ApJ*, 250, 254

Walter, F.M., Brown, A., Linsky, J.L. et al. 1987, *ApJ*, 314, 297

Weaver, Wm. Bruce 1987, *ApJ*, 319, L89

Weise, P., Launhardt, R., Setiawan, J., Henning, T. 2010, *A&A*, 517, A88

Welty, A.D., Ramsey, L.W., Iyengar, M. et al. 1993, *PASP*, 105, 1427

Welty, A.D. & Ramsey, L.W. 1994a, *ApJ*, 435, 848

Welty, A.D. & Ramsey, L.W. 1994b, *AJ*, 108, 299

Wichmann, R., Torres, G., Melo, C.H.F. et al. 2000, *A&A*, 359, 181

Wickramasinghe, D.T., Tout, C.A., Ferrario, L. 2014, *MNRAS*, 437, 675

Wolk, S.J. & Walter, F.M. 1996, *AJ*, 111, 2066

Zwintz, K. 2008, *ApJ*, 673, 1088

Zwintz, K. & Steindl, T. 2022, *Front. Astron. Space Sci.* 9:914738 doi: 10.3389/fspas.2022.914738

11. APPENDIX A: MEMBERS OF THE HP TAU MULTIPLE SYSTEM

The stars HP Tau/G2, KPNO 15, HP Tau, and HP Tau/G1 are discussed in Section 5, and XEST 08-033 in Section 4. The numbers below refer to Table 1.

1: *FF Tau*: This was first recognized as a T Tauri star by B.F. Jones & G.H. Herbig (1979). G.J. Herczeg & L.A. Hillenbrand (2014) has determined an optical spectral type of K8. Identified as a Taurus member by B.F. Jones & G.H. Herbig (1979) FF Tau is a binary, detected by Simon et al. 1987 M. Simon et al. (1987) and A. Richichi et al. (1994), with a separation of 36.3 mas and a ΔM 1.03 mag in a K_p filter (A.L. Kraus et al. 2011). A dynamical mass determination by A.C. Rizzuto et al. (2020) yielded a total system mass of $1.129 \pm 0.027 M_{\odot}$.

2: *XEST 08-049*: This is a variable X-ray source (M. Güdel et al. 2007), also known as 2MASS J04355286+2250585. It was identified as a young star by L. Scelsi et al. (2007, 2008). K.L. Luhman et al. (2017) determined a spectral type of M4.25.

3: *HQ Tau*: G.J. Herczeg & L.A. Hillenbrand (2014) have determined a spectral type of K2.0. K. Pouly et al. (2020) has studied accretion in the star, and find that a Kepler-K2 light curve exhibits a period of 2.424 d. They also suggest that the star may be a spectroscopic binary. Long term monitoring with KELT shows a dipper light curve (J.E. Rodriguez et al. 2017).

5: *KPNO 9*: Also known as 2MASS J04355143+2249119. This is a brown dwarf with spectral type M8.5V discovered by C. Briceño et al. (2002).

6: *XEST 08-033*: Also known as 2MASS J04354203+2252226. This is a medium-strong $H\alpha$ star from Strom et al. (1986) and identified as an X-ray source by M. Güdel et al. (2007). K.L. Luhman et al. (2017) finds a spectral type of M4.75 and Y.-X. Guo et al. (2019) suggest M6. Discrepant radial velocity measurements from APOGEE suggests that the star is a spectroscopic binary.

8: *HP Tau* was discovered as a variable star by G.S. Badalian (1961) and recognized as an $H\alpha$ emission star, Lk $H\alpha$ 258, by G.H. Herbig & N.K. Rao (1972). It has an optical spectral type of K4 according to G.J. Herczeg & L.A. Hillenbrand (2014), who estimate a mass around $1 M_{\odot}$. Our spectrum, which also indicates a K4 spectral type, shows strong $H\alpha$ emission with $W(H\alpha) = 9.1 \text{ \AA}$, and it also has $H\beta$ in emission. C.-L. Lin et al. (2023) present a LAMOST spectrum, which shows only $H\alpha$ in emission, and they determine a low accretion rate. Our near-infrared spectrum shows clear Brackett γ emission and strong Paschen β , γ , and δ lines in emission. It is a close binary found through lunar occultation with projected separation 17 ± 1 mas by A. Richichi et al. (1994), which corresponds to ~ 3 AU at the distance of the star. A.M. Cody et al. (2022) examined the K2 light curve which shows it is an aperiodic dipper, with a characteristic timescale of variability of 42.09 days and a normalized flux amplitude of 0.26. A. Garufi et al. (2025) note that HP Tau has a very high 2 cm flux that deviates significantly from a relation between free-free emission and mass accretion rate, and speculate that it might have undergone a recent episode of high accretion, or that the radio flux is dominated by synchrotron emission. Our $850 \mu\text{m}$ observation reveals a ~ 100 mJy source, indicating a circumstellar mass of $\sim 0.01 M_{\odot}$ of dust and gas.

9: *HP Tau/G3*: G3 was identified as a T Tauri star by M. Cohen & L. Kuh (1979), and G.J. Herczeg & L.A. Hillenbrand (2014) determined a spectral type of M0.6. It was found to be a close binary by A. Richichi et al. (1994), and A.L. Kraus et al. (2011) measured a separation of 30.5 ± 1.5 mas, corresponding to a projected physical separation of about 5 AU, and a magnitude difference at K-band of 1.44. A.C. Rizzuto et al. (2020) determined a total dynamical mass of the system of $1.005 \pm 0.053 M_{\odot}$, a period of 27.34 yr and an eccentricity of 0.521. It is an X-ray source (M. Güdel et al. 2007).

11: *Haro 6-28* was identified as an $H\alpha$ emission star by G. Haro (1953). Its optical spectral type is M3.1 as determined by G.J. Herczeg & L.A. Hillenbrand (2014). Ch. Leinert et al. (1993) used speckle interferometry to resolve it as a 0.66 arcsec binary. A.M. Cody et al. (2022) analyzed its Kepler K2 light curve and found a period of 21.56 days with a normalized flux amplitude of 0.23.

12: *2MASS J04355760+2253574*: This star was identified as a young very low mass object with spectral type M5 by S. Guieu et al. (2006). It is a periodic dipper with a period of 7.81 day and a normalized flux amplitude of 0.23 mag (A.M. Cody et al. 2022). On an HST image (Figure 21) it is seen to display the shadow of an edge-on disk with two illuminated lobes with a width of ~ 240 AU (Figure 26).

12. APPENDIX B: PROPER MOTIONS OF WALKAWAY STARS WITH DIFFERENT GROUP VELOCITIES

When a multiple system breaks up, momentum is conserved. If the velocities are known, one can determine the mass ratio. We deduced in Section 4 that G2 is ~ 1.5 times more massive than KPNO-15. However, this is sensitively

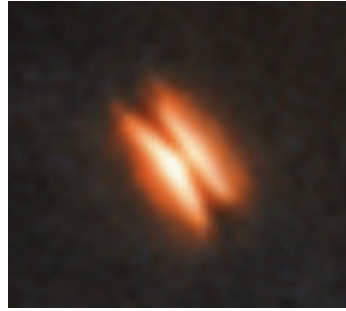


Figure 26. The M5 star 2MASS J04355760+2253574 has a $\sim 1.5''$ edge-on disk shadow bifurcating a compact reflection nebula, as revealed on the HST image seen in Figure 21. North is up and east is left.

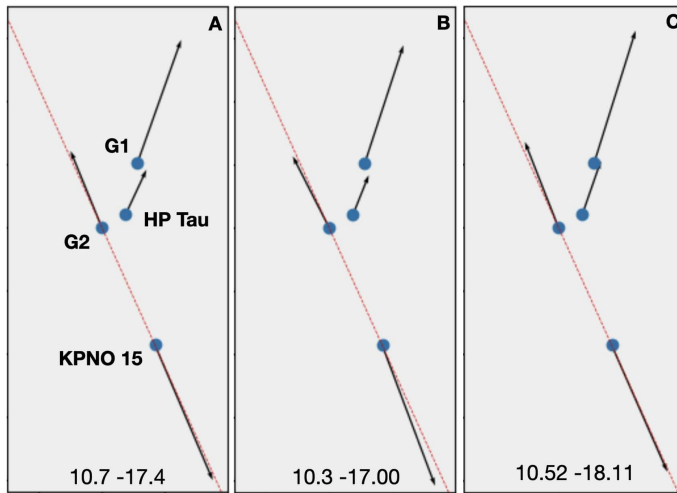


Figure 27. The measured proper motions of the three walkaway stars (incl. HP Tau which, although not formally a walkaway star, has a fairly large proper motion) relative to the rest frame of the molecular cloud depend sensitively on what group velocity is measured for the stars in the group. The panels show different determinations, A shows the Gaia DR2 solution of R. Kerr et al. (2021), B is the Gaia DR3 solution of K.L. Luhman (2023), C is our Gaia DR3 solution based on 7 closeby stars with small proper motions. The red line is a straight line through G2 and KPNO 15. The importance of choosing the correct rest frame is that the derived mass ratio for a walkaway pair is affected. The figure is 2.5×5 arcmin.

dependent on the correction of the Gaia proper motion by the group velocity. While the relative *angle* of the motion of two stars can be derived merely by subtracting the two observed Gaia vectors, the *ratio* of the velocities depends on the group velocity. In Figure B1 we show the vectors of the four walkaway stars when corrected for different group velocities. In Panel A the group velocity of R. Kerr et al. (2021) was determined from stars in B213 and L1536, Panel B shows the result of applying the group velocity of K.L. Luhman (2018), Panel C is our solution based on 7 nearby stars with small proper motions. In case A, the velocity ratio of G2 and KPNO 15 is 0.56, for case B, it is 0.53, and for case C it is 0.66. The mass ratio of G2 to KPNO 15 thus ranges from 1.52 to 1.89.

13. APPENDIX C: IS G2 PULSATING?

G2 was observed for 84 days by the K2 mission (Figure 28-top), much longer than with TESS (Figure 8). Based on the K2 data, L.M. Rebull et al. (2020) and A.M. Cody et al. (2022) determined two almost identical periods, $P_1=1.1978$ d and 1.222d. These two distinct periods can be explained by two separate, large spot groups at slightly different latitudes in a star with differential rotation. The photometric variation indicates that at the beginning of the K2 light curve spot group A, with $P(A) = 1.1978$ days, dominates. In the middle section (dashed box), group A is gradually fading away, while simultaneously spot group B, with $P(B) = 1.222$ days, grows, and in the final section of the light curve group B is dominant.

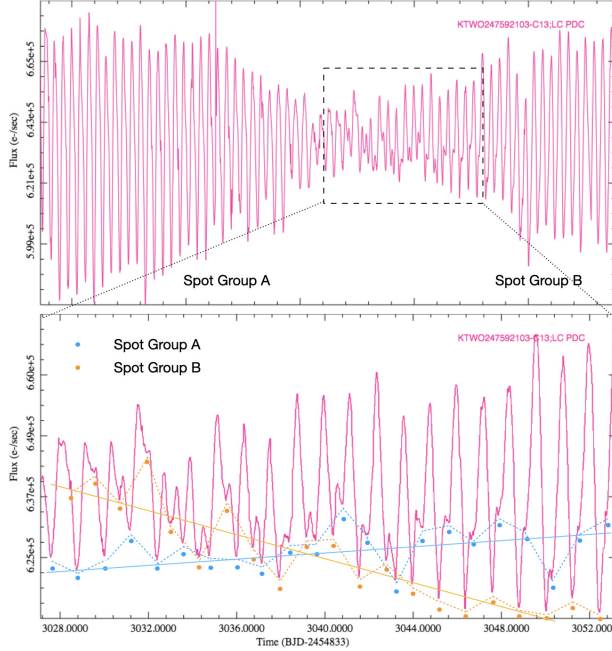


Figure 28. The light curve of G2 as observed by the Kepler K2 mission. The upper panel shows the entire light curve observed between March 9 and June 1, 2017, and the lower panel shows 26 days covering the transition phase when spot group A (blue dots, period 1.1978 days) shrinks and the absorption from spot group B (orange dots, period 1.222 days) becomes dominant.

However, the light curve shows a feature that is difficult to explain by two spot groups with slightly different rotation periods, namely the bottleneck in the middle of the light curve. The lower envelope will rise when the spots shrink. But the upper envelope should always reach maximum light whenever the two spot groups are on the same side facing away. Only when they are precisely opposite each other would the upper envelope fade, especially if the spot groups have grown very large, part of one is always seen. It is also required that the two spot groups are both changing at the same time to explain the rise of the lower envelope. Such a situation is possible, but perhaps not common.

On the other hand, such bottle-necks are commonly seen in double-mode radial pulsations in a star, with two periods creating a beat. And we note that high-resolution spectra of the H α line of the merger FK Com show variability of the profile that has been ascribed to non-radial oscillations excited by the recent merging of two stars (A.D. Welty & L.W. Ramsey 1994a).

A simple pulsating model with periods of 1.1978d and 1.222d will reproduce the large scale behavior seen in Figure 8-top while two spot groups with the same periods will reproduce the detailed structure seen in Figure 8-bottom.

Most pre-main sequence stars that are known to pulsate inhabit the δ Scuti instability strip (e.g. K. Zwintz 2008), but there are seven types of pulsations recognized in young stars, either observationally or theoretically (K. Zwintz & T. Steindl 2022). G2 is too cool to inhabit the instability strips of δ Scuti and γ Doradus stars, the two most common PMS pulsators. It is, however, close to the cool edge of the γ Doradus stars, and in fact a few pulsators (not young) are known to inhabit that region in the HR-diagram (L.A. Balona 2018).

The semi-amplitude observed in G2 is \sim 5%, and that is more than has been seen in any Gamma Doradus stars (D. Bowman & L. Bugnet 2026). Also, the pulsation-like light curve seen by K2 is not seen in the TESS data (Figure 8). Overall, it seems unlikely that G2 is pulsating.

14. APPENDIX D: V838 MON AND V1309 SCO

The leading interpretation of V838 Mon is that two young (<25 Myr) main sequence binary components of masses $\sim 1.5 M_{\odot}$ and ~ 0.1 - $0.5 M_{\odot}$ merged (N. Soker & R. Tylenda 2003). The star has an unresolved B3V companion and is also part of a small cluster of young B-stars (U. Munari et al. (2002), M. Afsar & H.E. Bond (2007)). The aftermath of the spectacular $\sim 10^6 L_{\odot}$ eruption was followed in detail spectroscopically and photometrically. Subsequent ALMA observations revealed a disk-like structure surrounding the star and determined a projected separation of ~ 150 AU to

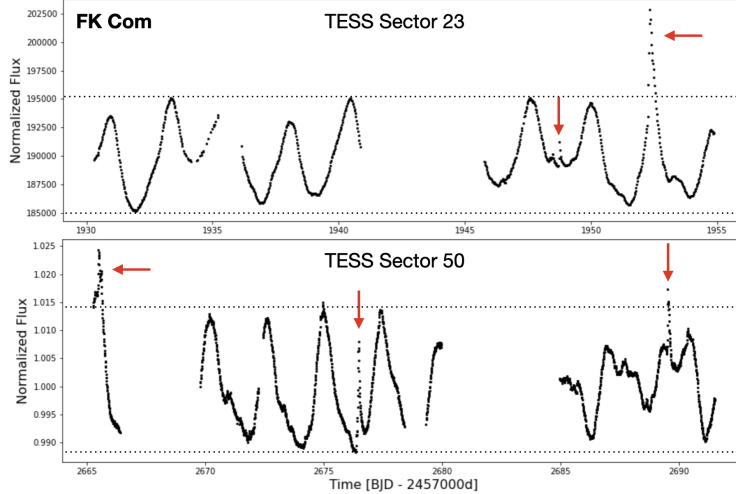


Figure 29. The light curve of FK Com as observed by TESS. The periodicity is well-established, but it is not clear whether the more detailed structure is due to the presence of a bright very nearby star or due to technical issues. The more structured variability around 2690 is most likely real. FK Com is a well-known flare star, and five flares are seen here, which suggests a rate of roughly one flare per every 8 days.

the B-companion, indicating that V838 Mon is the remnant of a binary merger in a triple system (T. Kamiński et al. 2021).

The eruption of V1309 Sco was extraordinarily well documented, with a ~ 10 yr light curve that covers the entire eruption (R. Tylenda et al. 2011), including several years before the outburst. The progenitor was a ~ 1.4 day contact binary with an exponentially decreasing period prior to the eruption. Analysis of the pre-outburst light curve indicates that the contact binary had a mass ratio of less than 0.1 (K. Stepień 2011). The luminosity of the star remained $> 10^4 L_\odot$ for a month during which $\sim 3 \times 10^{44}$ erg was radiated away (R. Tylenda et al. 2011). At the peak of the eruption V1309 Sco showed a near-infrared spectrum mimicking an F-giant (R.J. Rudy et al. 2008a), which quickly over the next month turned into a late M-giant (R.J. Rudy et al. 2008b; E. Mason et al. 2010). This evolution could be a signature of the expulsion of an expanding envelope from the star. Currently, 17 years after the eruption, V1309 Sco is a red giant, presumably due to expansion. Analysis of high resolution spectra show that during the eruption matter was expelled as dust-laden bipolar ejecta and that the star is surrounded by a doughnut of gas, which was produced during pre-outburst mass-loss episodes (E. Mason & S.N. Shore 2022). Far-infrared data from Herschel has confirmed cold dust a few thousand AU from the star (R. Tylenda & T. Kamiński 2016).

15. APPENDIX E: FK COM: H α EMISSION AND FLARES

The strong H α line in FK Com has been studied by many observers, e.g., A.D. Welty et al. (1993), D.P. Kjurkchieva & D.V. Marchev (2005), and H. Korhonen et al. (2009). It has a complex structure with a broad absorption ~ 1000 km s $^{-1}$ wide overlaid by a double peaked emission reaching above the continuum with the red and blue components varying in strength in anti-phase, resulting in an absorption core that shifts between blue- and red-shift. Given the similarity between G2 and FK Com, it is likely that G2's H α profile would be similarly varying if monitored.

FK Com, with a $v\sin i$ of ~ 160 km s $^{-1}$, is also the most active of the little group of FK Com-type stars. It is a well-known flare star and the TESS light curve suggests that it has a flare roughly once every 8 days. Flares have been observed photometrically at optical wavelengths (...), spectroscopically in the Balmer lines (an H α superflare was detected by J.M. Oliveira & B.H. Foing 1999), in X-rays (F. Favata et al. 1998), in the ultraviolet (T.R. Ayres et al. 2016), and a major flare was detected at millimeter wavelengths by J.B. Lovell et al. (2024). We note that G2 also shows flares (two flares are seen in the TESS light curve in Figure 8), and similarly the TESS light curves of HD 283572 show multiple (small) flares.

16. APPENDIX F: MERGERS AND FUOR ERUPTIONS

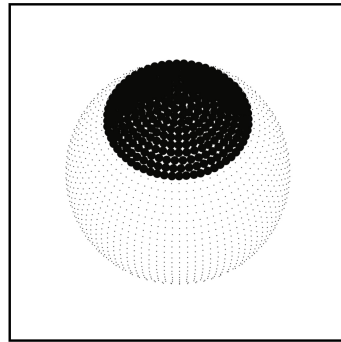


Figure 30. A model of the stellar photosphere of FU Ori from [P.P. Petrov & G.H. Herbig \(2008\)](#) based on stellar line profiles. The line profiles reveal a major polar starspot.

At the time of the eruptions, G2 and HD 283572 would have been much brighter, and would have been located in the general area of the FUors in the diagram in Figure 19. We here speculate whether some FUors could be the result of mergers.

At its most basic level a FUor is a young star that has undergone a major eruption that led it to be swollen and fast rotating and with an A-, F-, or G-type optical spectrum displaying prominent P Cyg line profiles from a cool wind (e.g., [G.H. Herbig et al. 2003](#)). In the near-infrared they have late-type spectra emitted by an accretion disk.

We note that when the V838 Mon merger took place, it was initially suspected of being a FUor based on the high velocity cool winds seen as P Cygni profiles at $H\alpha$ and the Sodium doublet, and the strength of Barium (e.g., [T. Kipper et al. 2004](#)), mimicking a FUor.

Herbig and Petrov, in a series of important but underappreciated papers, argue that the metallic line profiles of FU Orionis in optical high resolution spectra are well explained as originating in a very luminous, bloated, and fast rotating star with a major polar star spot, see Figure 30 and [G.H. Herbig \(1989\)](#), [P.P. Petrov & G.H. Herbig \(1992\)](#), [G.H. Herbig et al. \(2003\)](#), and [P.P. Petrov & G.H. Herbig \(2008\)](#). We are agnostic about whether these optical lines observed in FU Orionis originate in the star or from the inner disk, but merely note that if interpreted as having a photospheric origin then FU Orionis would be very similar to what would be expected from the recent merger of two low-mass stars.

As more and more eruptive events are discovered, the pioneering but now simple division into FUor and EXor eruptions ([G.H. Herbig 1977](#)) is becoming increasingly inadequate, and many erupting objects are found with a large range of characteristics (e.g., [L.A. Hillenbrand et al. 2021, 2022, 2023](#)), challenging their classification.

FUors, in the most inclusive sense of the term, can be formed from a variety of processes (e.g., [E.I. Vorobyov et al. 2021](#)). We suggest that stellar mergers can be added to those. Mergers will cause outbursts that are likely to differ due to individual circumstances, in particular the range of masses of the merging objects (stars, brown dwarfs, planets).

It is possible that G2 at the time of its eruption would have appeared as a FUor eruption, in which case G2 and HD 283572 would be post-FUors. If so, then the main difference between G2 as it is seen today and more recent FUors lies in its evolutionary stage, with FU Orionis being much younger and still surrounded by a large cool disk, while G2 erupted at a later stage and lost what remained of its circumstellar material in the merger explosion. Hence G2 does not show the late-type spectrum at near-infrared wavelengths which is characteristic of most FUors.

It is not known how long FUor eruptions preserve their characteristics. The longest-lasting FUor known, V883 Ori, erupted before 1888 ([K.M. Strom & S.E. Strom 1993](#)), yet still today has a luminosity of about $220 L_\odot$ ([E. Furlan et al. 2016](#)). FU Ori erupted in 1938 and brightened from $V \sim 16.5$ mag. to ~ 9.6 mag. Since then it has faded only ~ 0.7 mag. in V. The rate of decline, however, is variable (e.g., [M.A. Ibragimov 1993](#)), but if on average the decline stays constant, then it will take almost 1000 yr for FU Ori to fade to its original brightness. At the other extreme, V1057 Cyg has since its peak brightness around 1970 already faded by almost 4 mag. in V (e.g., [Zs. M. Szabo et al. 2021](#)).

We do not know when the eruption of G2 took place, other than it was less than 5600 yr, but at least in principle it could be as little as a few centuries.

We conjecture that G2 and HD 283572 once appeared as FUor eruptions and that, as a result of the significant energy release in the merger, the remaining parts of their accretion disks were lost. Subsequently the two stars would

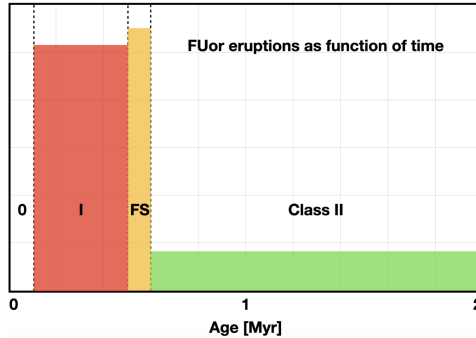


Figure 31. The distribution of FUor and FUor-like objects as a function of time. The figure assumes that the Class 0 phase lasts about 0.1 Myr, Class I about 0.4 Myr, flat-spectrum about 0.1 Myr, and Class II about 2 Myr. Data from C. Contreras Peña et al. (2025).

appear as bloated luminous stars that began the internal restructuring corresponding to a star with the combined mass of the precursor binary. This will be completed on a Kelvin-Helmholtz timescale, although the peculiarities that draw our attention today likely would disappear much earlier.

Most FUor eruptions occur during the protostellar phase (C. Contreras et al. 2025, in prep.) and consequently they very often have substantial accretion disks leading to a strong infrared excess. Although such outbursts were originally identified among visible stars (G.H. Herbig 1977), the most recent work shows that they are far more common during the protostellar phase. Figure 31 shows the distribution of FUors and FUor-like objects as a function of time from the major compilation of young eruptive stars by C. Contreras Peña et al. (2025), who tabulated all known major YSO outbursts, including 62 (at the time of writing) FUors and FUor-like objects. This is consistent with the finding through numerical simulations that triple breakups are much more frequent during the earliest evolutionary phases.

We wish to stress that we do not suggest that *all* FUors are formed in mergers, just that it is an additional viable explanation for strong outbursts in young stars.